

Chapter 8

Other Studies

This Chapter describes the analysis of three distinct aspects of the QSO spectra studied in this thesis.

Section 8.1 details a serendipitous observation which may indicate structure in the Lyman α emission lines on scales not seen previously, and follows through the possible consequences. Section 8.2 discusses the validity of the assumption that individual QSO sightlines are representative of large volumes of high-redshift space. Section 8.3 describes the search for evidence of metal line absorption in the Lyman α forest systems.

8.1 Possible Structure in the Lyman α Emission Line

When examining the echelle spectra of all three QSOs observed with UCLES, Q2206–199N (Pettini *et al.*, 1990), Q1101–264, and Q2348–147, a peculiar but consistent pattern comes to light. The blue wings of the Lyman α emission lines, where they are not heavily absorbed by strong lines, contain apparent weak absorption features with unusual, broad profiles. The shapes of many of these features do not resemble Voigt profiles, being triangular, cusp-like, or strongly asymmetric. Some of these shapes are illustrated in Figure 8.1.

The triangular, cusped, and asymmetrical shapes can be produced by blended Voigt profiles of appropriate strengths and velocity separations, combined with some level of noise, but seeing several such shapes in the Lyman α emission line wing of three different objects and nowhere else is suggestive of a common phenomenon. If broader regions of spectrum are considered, the presence of these unusual shapes gives the line wing a distinctive “lumpy” appearance. Several sections of spectrum showing the unusual appearance of the line wing in the three objects are shown in Figure 8.2. Sections of spectrum far from the emission lines in each object are shown in Figure 8.3 for comparison. To remove the highest frequency noise components, all these spectra have been smoothed slightly (with a 0.07 \AA FWHM gaussian filter) compared with the spectra presented in Appendix A.

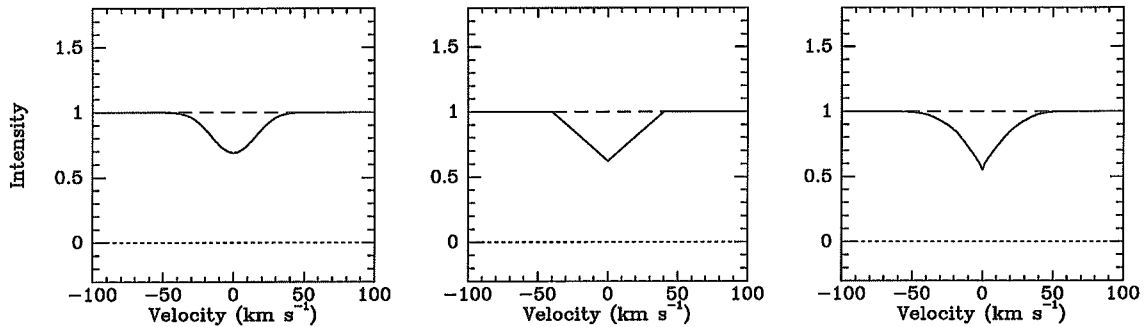


Figure 8.1 Diagram showing some different absorption profile shapes present in the spectra of the QSOs 2206–199N, 1101–264, and 2348–147. *Left:* A Voigt profile; this profile is for Lyman α with $b = 30 \text{ km s}^{-1}$ and $\log N = 13$. *Centre:* A triangular profile. *Right:* A cusped profile; the latter two profiles can be produced in absorption only by blending of several components with fortuitous strengths and velocity offsets.

Note in particular in Figure 8.2 the shape of the absorption features at ~ 4231 , 4234 , 4240 \AA in Q2206–199N, $\sim 3775 \text{ \AA}$ in Q1101–264, and ~ 4707 , 4714 , 4772 \AA in Q2348–147. Also note the general shape of the spectra (ignoring the obvious strong absorption lines), with many extended fluctuations below the fitted continuum that are not clearly associated with single absorption lines, and a few areas significantly above the continuum for several pixels. There are ~ 2.5 pixels per resolution element, so fluctuations covering ≥ 4 –5 pixels are significant. (The presence of extended fluctuations above the adopted continuum could be used to argue that the continuum has been placed too low.) If these regions are compared with those shown in Figure 8.3—where there are absorption features with single Voigt profile shapes or simple blends of these, and a relatively flat (though noisy) continuum—a difference in the overall character of these portions of spectrum can be noticed.

It is worth noting that awareness of the unusual shapes of the Lyman α emission line wings first surfaced when fitting continua to the spectral orders. This was possible because of the interactive approach taken with continuum fitting. An automated procedure, such as the one described in Section 2.1.1, would not reveal any such unusual structures in the spectrum. Since most researchers have tended to use automated continuum fitting methods, it is not surprising that nothing like the structures examined here has been reported previously.

There are three possible explanations for these observations:

1. The random positioning of absorption lines in the spectra and the vagaries of the noise are such that they generate the unusual overall appearance of the emission line wings in each object.
2. Absorbing clouds physically near the background QSOs, or possibly even in the broad line emitting region itself, are affected by their environment so that they form unusually shaped composite profiles extending over large velocity spans.

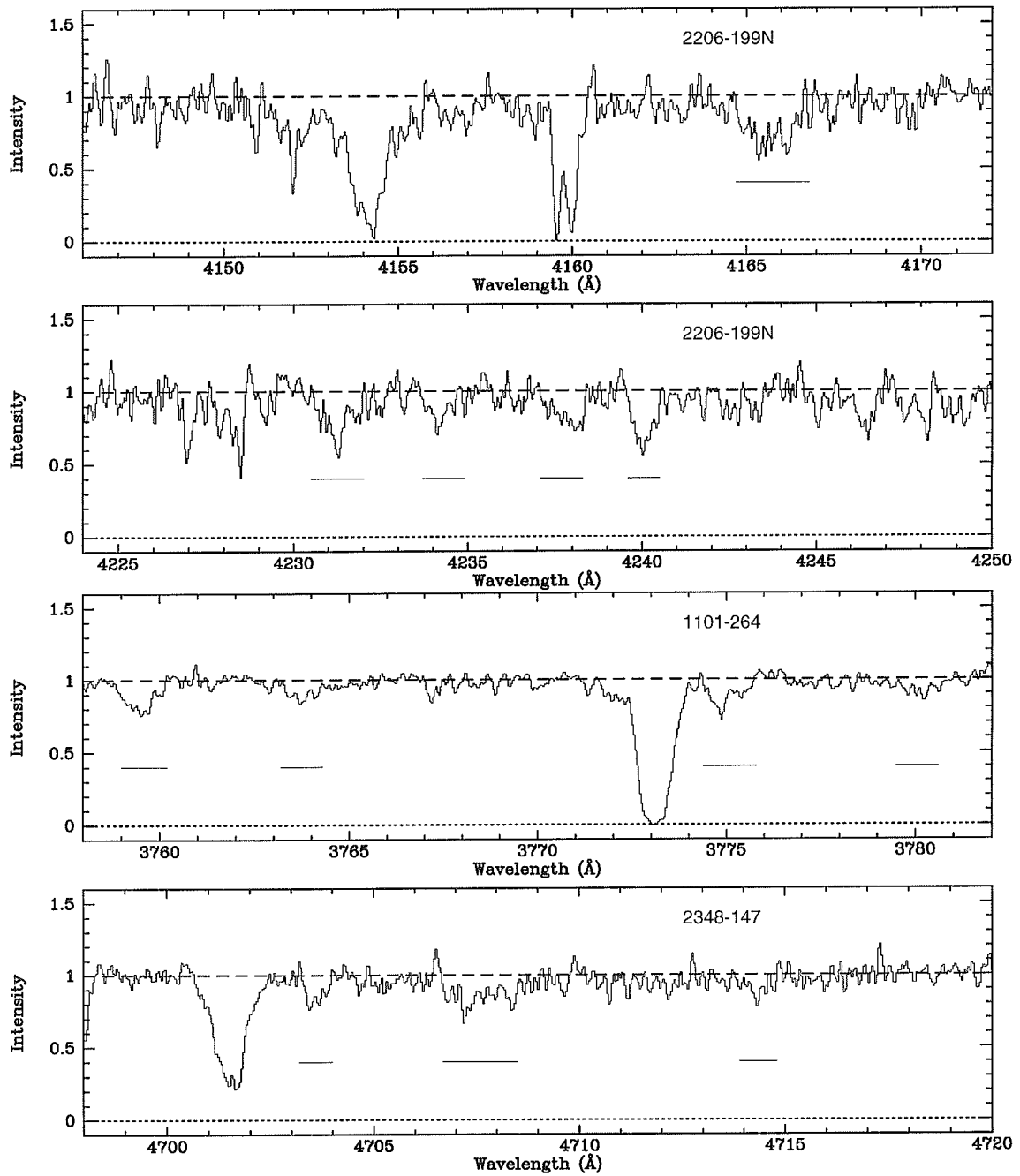
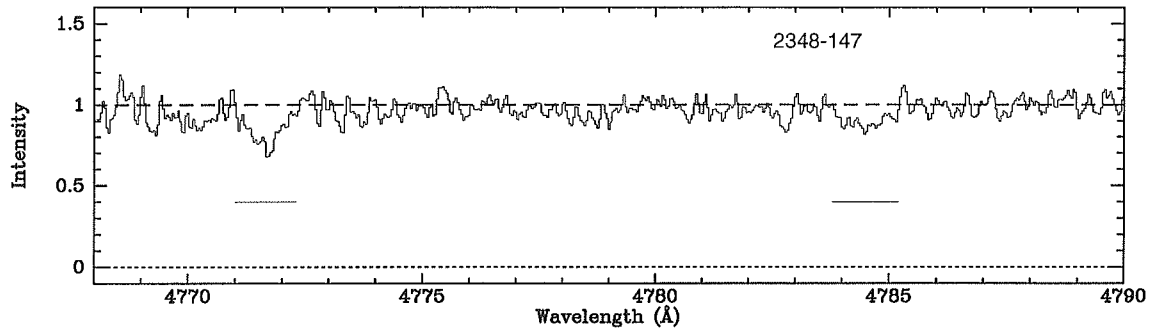
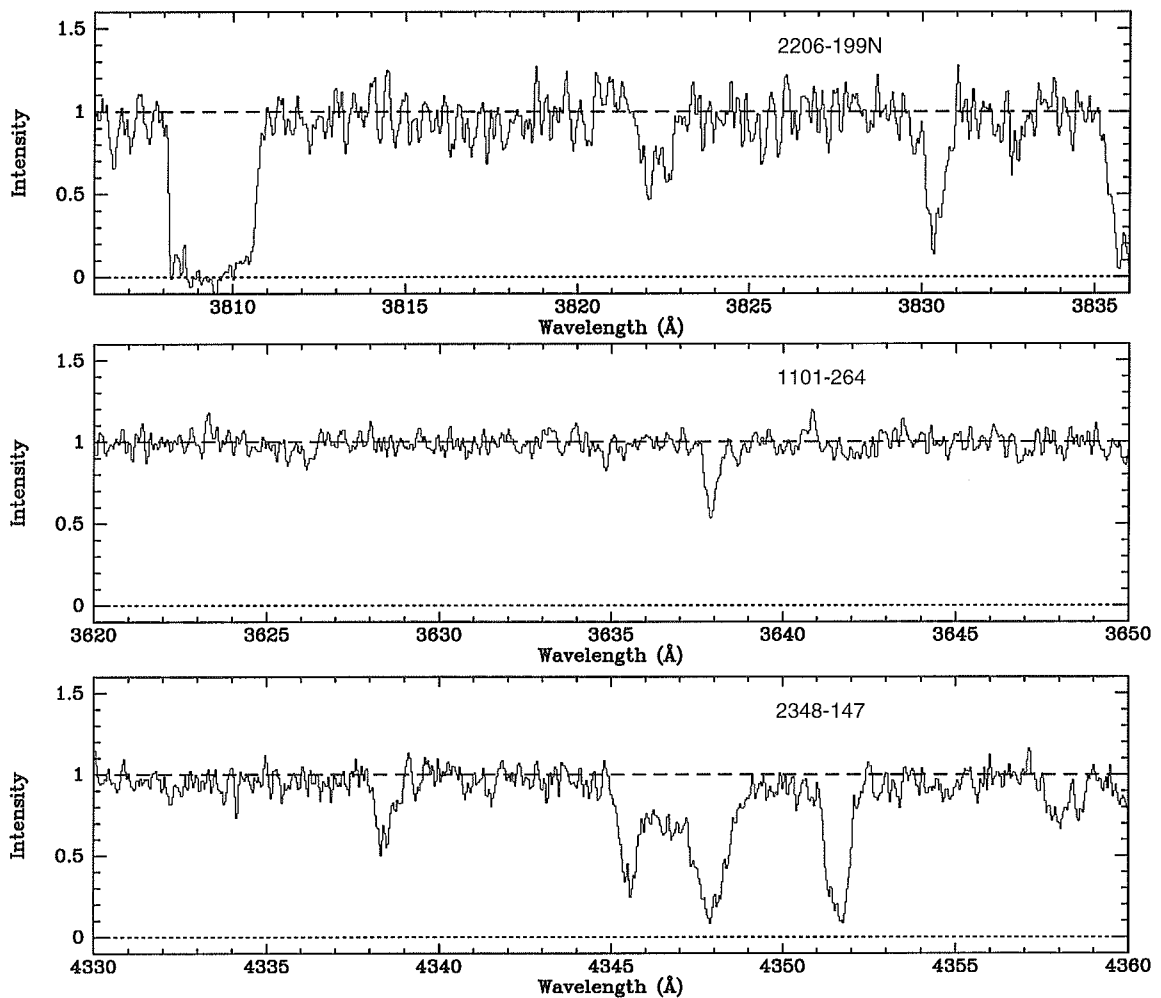


Figure 8.2 Possible structure in the Lyman α emission line of QSOs 2206–199N, 1101–264, and 2348–147. The horizontal bars mark regions with unusually shaped features. See Section 8.1 for a full description.

Figure 8.2 Possible emission line structure (*continued.*)Figure 8.3 Sections of the spectra of QSOs 2206–199N, 1101–264, and 2348–147 far from the Lyman α emission line, showing few or none of the unusual features shown in Figure 8.2. See Section 8.1 for a full description.

3. The underlying emission line is not smooth, but possesses structure on a velocity scale similar to the typical separations of the supposed unusual absorption features. The features would then be inherent in the emission line profile, not absorption at all.

These three possibilities, followed by an observational method of testing which might be true, are discussed in the sections below.

8.1.1 Random Features

The first possibility, though difficult to eliminate completely, is rendered unlikely by the presence of such structures in the emission line wings of all three objects. Additionally, no such structures are seen in Ed Jenkins' Cloudy Night QSO, which has a similar S/N ratio in the continuum to the three real objects.

The CNQ spectrum was produced with a smooth emission line and no particularly unusually-shaped absorption features are seen in it—indeed one is struck by the general impression that the CNQ absorption lines are *more* like pure Voigt profiles than the lines in the real objects. This is despite the very high density of absorption lines in the CNQ spectrum (which has been commented on in Section 3.6) and the resulting high likelihood that lines will be blended. The one obvious “lumpy” region in the CNQ spectrum (3998–4006 Å) contains features which are plainly single Voigt profiles and none of the triangular or cusped shapes (see Figure A.3).

Unfortunately, it is very difficult to perform any meaningful statistical analysis of the significance of these observations, especially since the classification of “unusualness” is somewhat subjective.

8.1.2 Physically Disturbed Absorption

The second possibility is that the unusual features observed in the Lyman α emission line wings are caused by absorption in clouds which are somehow physically disturbed, or which do not fully cover the emission line region, making the line profiles non-Voigtian.

It is known that the number of Lyman α clouds in a given column density (or equivalent width) range per unit redshift increases with redshift, but that the trend in individual QSO spectra is the opposite (the proximity effect, see Section 1.5.4). This provides evidence for the influence of QSOs over the surrounding regions of space—the radiation from the QSO significantly increases the ionisation of gas over comoving distances of $\sim 5\text{--}10h^{-1}$ Mpc, thereby reducing the column density of neutral hydrogen (Bajtlik *et al.*, 1988).

To test whether increased ionisation could be a plausible cause for the unusual features, the velocity offsets and comoving distances between the Lyman α emission lines and the areas were calculated and are shown in Figure 8.2. Of course, the distances shown in Table 8.1 assume the velocity differences are caused solely by the Hubble flow. If the absorbing clouds are outflowing or infalling at significant velocities, the distances would be smaller or greater, respectively.

Table 8.1 Velocity differences v and comoving distances d between the Lyman α emission line peak and the spectral regions showing unusual absorption features (Figure 8.2). The comoving distances are calculated for an Einstein-de Sitter cosmology.

Object	$\lambda_{\text{em}}(\text{Ly } \alpha)$ Å	λ Range Å	v Range km s^{-1}	d Range h^{-1} Mpc
Q2206–199N	4320	4146–4172 4224–4250	12080–10270 6660– 4860	66.0–55.9 35.9–26.1
Q1101–264	3818	3758–3782	4710– 2830	26.9–16.1
Q2348–147	4790	4698–4720 4768–4790	5760– 4380 1380– 0	29.4–22.3 7.0– 0.0

If no outflow is assumed, then it seems unlikely that any influence from the QSOs would reach as far as most of the distances listed in Table 8.1. Mere increased ionisation would not produce the non-Voigt-profile features seen in the spectra in any case—some more violent physical disruption would be needed, such as a streaming of gas along the line of sight, perhaps caused by radiation pressure. Such a scenario is highly unlikely so far from the QSO. (Also, it is not clear if even such violent motions will reproduce the shapes seen in the spectra.)

A more natural alternative is that there may be absorbing clouds physically close to the QSO, which are outflowing and also physically disturbed in some manner by their proximity to the radiation source. The broad line region (BLR) is known to be composed of more or less discrete clouds of emitting gas (Osterbrock and Matthews, 1986, and references therein). One possibility is that some of these clouds, on the nearer side, are absorbing some of the radiation from the clouds on the far side, which are emitting in our direction.

The following facts are known about the BLR clouds:

- The BLR clouds are optically thick in Lyman α and therefore emit their radiation anisotropically, back towards the central ionising source (Ferland and Netzer, 1979; Ferland and Truran, 1981).
- The covering factor of these clouds—the fraction of the sky covered by the clouds—as seen from the central source, is $\Omega/4\pi \sim 0.05\text{--}0.15$ (Baldwin and Netzer, 1978; Smith *et al.*, 1981; Oke and Korycansky, 1982). (Ω is the solid angle subtended by all the clouds at the central source, in steradians.)
- The temperature of the clouds is most probably $\sim 10^4$ K, corresponding to a thermal Doppler width of $\sim 10 \text{ km s}^{-1}$ (Capriotti *et al.*, 1981; Osterbrock and Matthews, 1986; Peterson, 1995).
- To produce the relatively smooth AGN broad line profiles observed at resolutions of $\sim 1 \text{ \AA}$, there must be $\gtrsim 10^4$ such clouds in the BLR (Capriotti *et al.*, 1981; Atwood *et al.*, 1982).
- There is some evidence for a net infall of clouds in the BLR of AGNs and no

observations yet seem to indicate any outflow¹ (Peterson, 1993, and references therein).

The fact that the BLR clouds emit anisotropically back towards the central source means clouds closer to us are ideally positioned to absorb the radiation from those clouds which emit along our line of sight. This is illustrated schematically in Figure 8.4. The optical depth which leads to the anisotropic radiation also means that any absorption by such clouds is complete, provided they cover the emitting clouds. However, if the clouds are uniformly distributed about the central source, only ~ 0.1 of the emitting region (from our point of view) will be covered, since the central-source covering factor $\Omega/4\pi$ of the clouds is of this order. This line-of-sight covering factor may be significantly different if the distribution of the BLR clouds is not azimuthally symmetric, *e.g.* a toroidal distribution.

A complication arises because the clouds have line-of-sight velocities which may span a velocity range of up to $\sim 10\,000\text{ km s}^{-1}$. A Lyman α photon emitted by one cloud will only be absorbed in an intervening cloud if the velocity difference between the clouds is of the order of the internal velocity dispersion of the gas, or smaller.

It is clear that clouds closer to us do not fully cover—in either space or velocity—the clouds emitting in our direction, at least in the majority of QSOs. Such a configuration would produce line profiles similar to those observed in broad absorption line (BAL) QSOs, which are relatively rare². Therefore there are some regions from which the Lyman α photons reach us unimpeded, either because they encounter no other clouds or because any clouds encountered are not near zero velocity relative to the emitting cloud.

At most, then, a fraction of the emission at any given velocity shift will be absorbed. This partial covering of the radiation source may produce noticeable features in the emission line, similar to those observed in the QSOs studied here. Such features will not be simple Voigt profiles because of the low line-of-sight covering factor. They would also be more visible in the extreme wings of the emission line, where the number of clouds of appropriate velocity is small, so they do not fully span a range of velocity and blend into a smooth profile.

The conclusion of no net outflow of BLR material, if correct, implies the number of clouds positioned to absorb the blue wing of the emission line is less than or equal to the number which can absorb the red wing. In this case, the optimal number of clouds for observing any effects of their absorption would occur further from the systemic redshift (in velocity) in the red wing than the blue wing. However, it is known that the peaks of high-excitation broad lines (such as Lyman α) are systematically blueshifted with respect to the systemic redshift (defined by the narrow, low excitation emission lines, *e.g.* Mg II $\lambda\lambda 2796, 2803$, H I $\lambda 6562$) by $\gtrsim 1000\text{ km s}^{-1}$ (Gaskell,

¹If it is true in general that BLR clouds are infalling, then the broad line emission of AGNs may be a relatively short-lived phenomenon.

²The broad absorption features seen in BAL QSOs are thought to be caused by absorbing material located far outside the BLR, but still within the QSO environment (Weymann *et al.*, 1981).

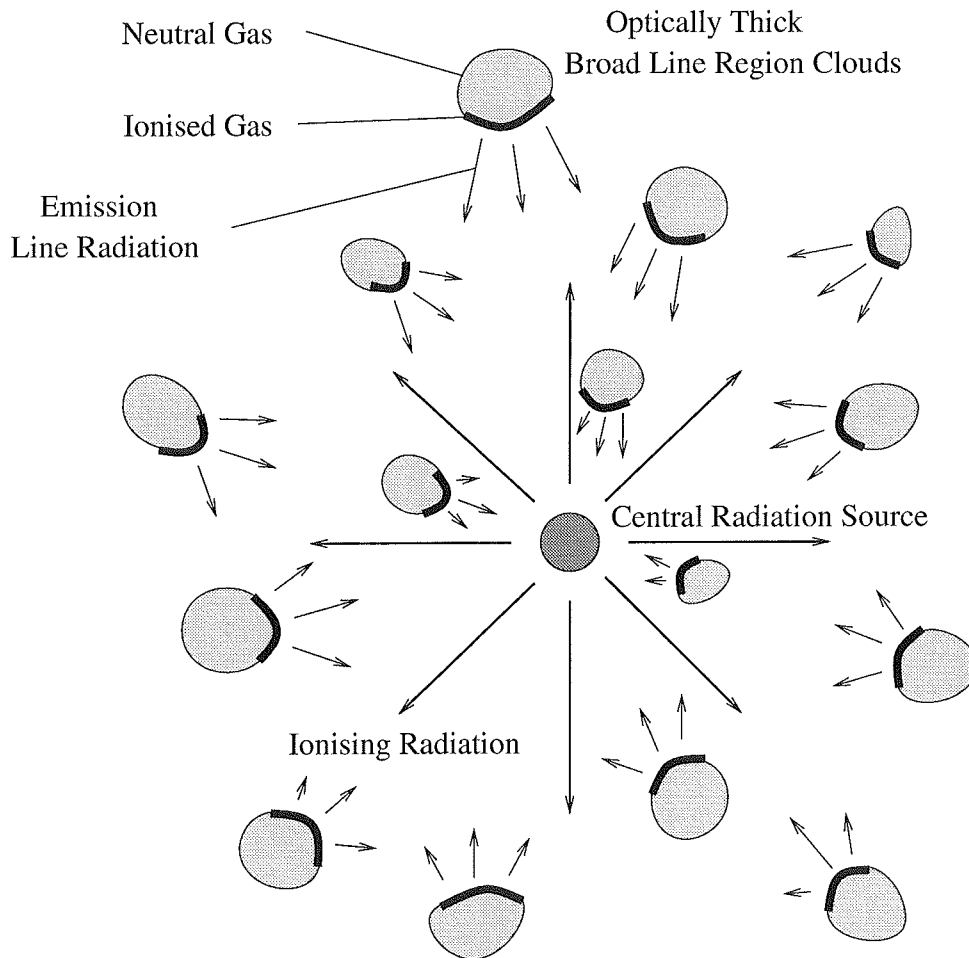


Figure 8.4 A “cartoon” illustration of the broad line region of a QSO. The central radiation source is usually assumed to be a massive black hole surrounded by an accretion disc. The central source emits a large amount of ionising radiation ($h\nu > 13.6\text{ eV}$), which ionises the facing edges of the surrounding, optically thick, clouds. The ionised parts of the broad line clouds emit anisotropically, back towards the central source. Broad emission lines are therefore predominantly composed of emission from clouds on the far side of the central source. Note that the diagram is not to scale: In reality there are $\gtrsim 10\,000$ broad line clouds, which are small and moving with speed $\sim 1000\text{--}5000\text{ km s}^{-1}$ around the central source. The breadth of the broad emission lines is caused by the resulting Doppler shifts.

1982; Espey *et al.*, 1989). If the position of BLR cloud absorption features is measured relative to the broad line, the redshift offset exaggerates the difference further. The possibility of using the expected resultant asymmetry to test this hypothesis is discussed in Section 8.1.4.

8.1.3 Emission Line Structure

The final possibility, that the features in the emission line wings are caused by structured emission, is also intriguing. To assess the significance of a possible detection of substructure in the Lyman α lines of QSOs, a brief review of the structure of active galaxy emission lines is in order.

There is substantial evidence for substructure in the narrow forbidden emission lines of active galaxies, based on the shapes of the line profiles. In a sample of 42 Seyfert and H II galaxies, Whittle (1985) found asymmetries in the [O III] $\lambda 5007$ lines, indicating a number of components. Cecil *et al.* (1990) found similar structure in the [N II] $\lambda\lambda 6548, 6583$ emission profiles of the Seyfert galaxy NGC 1068.

Direct deblending of broad emission lines into two or more components has been done for the H β line in the type 1 Seyfert galaxy NGC 5548 by Peterson *et al.* (1990) and Wamsteker *et al.* (1990), for the H α (H I $\lambda 6562$) line in the same object by Dietrich *et al.* (1993), and for the C IV $\lambda 1549$ line³ by Wamsteker *et al.* (1990). Generally, the broad line profiles consist of a “core” component of velocity width $\sim 5000 \text{ km s}^{-1}$ FWHM and a “base” component of velocity width $\sim 10000 \text{ km s}^{-1}$ FWHM, blueshifted by $\sim 2000 \text{ km s}^{-1}$ with respect to the core component. There is also a narrow component—which shares many properties with the narrow forbidden lines and arises in the narrow line region of the object—and evidence for up to two other, weaker components in some lines.

Wills *et al.* (1993) and Brotherton *et al.* (1994) have done similar decompositions of the C IV $\lambda 1549$, C III] $\lambda 1909$, and Mg II $\lambda 2798$ lines⁴ in a sample of 123 QSOs. In this case, there is a core component of velocity width $\sim 2000 \text{ km s}^{-1}$ FWHM and a base component of velocity width $\sim 7000 \text{ km s}^{-1}$ FWHM, blueshifted by $\sim 1000 \text{ km s}^{-1}$ with respect to the core component. This similarity of structure between type 1 Seyfert galaxies and QSOs hints at possible relationships between the velocity structures of the emitting gas in these objects.

Structures on smaller scales have been revealed by the reverberation mapping technique, first described quantitatively by Blandford and McKee (1982) and reviewed by Peterson (1993). This technique relies on the UV and optical time-variability of AGNs, in particular the fact that the emission line variability appears to be driven by changes in the continuum intensity, which occur on timescales of a few days. Assuming the emission line region is excited by photoionisation from the core, the light-curve of emission line intensity versus time is then the convolution

³This line is a blend of the C IV $\lambda\lambda 1548, 1550$ doublet. When the doublet appears as a broad emission line it cannot be resolved into its two components.

⁴This line is a blend of the Mg II $\lambda\lambda 2796, 2803$ doublet. Like the C IV $\lambda\lambda 1548, 1550$ doublet, the components cannot be resolved when they form a broad emission line.

of the continuum light-curve and a geometry-dependent transfer function. Given enough observations, the transfer function can be calculated and the geometry of the broad line region (BLR) constrained.

While a full, three-dimensional mapping of an active galaxy BLR has not yet been achieved, time-variability studies of the type 1 Seyfert galaxies NGC 5548 by Stirpe *et al.* (1988), Peterson *et al.* (1990), and Stirpe and de Bruyn (1991), Arakelian (Akn) 120 by Korista (1992), and 3C 390.3 by Veilleux and Zheng (1991) have revealed components in broad emission lines by observations of the different amplitudes of their intensity variations. The components seen in the H α and H β (H I λ 4861) lines of NGC 5548 are separated by $\sim 4000 \text{ km s}^{-1}$, and those in the H β lines of Akn 120 and 3C 390.3 by $\sim 2000 \text{ km s}^{-1}$.

If the QSO observations presented here do show emission line structure, the scale of the features imply velocity differences of $\sim 150\text{--}350 \text{ km s}^{-1}$ between clumps of emitting material. This is an order of magnitude smaller than the structures seen in the Seyfert galaxies, but the Seyfert galaxy observations were all made with much lower resolutions, 4 \AA for NGC 5548 and 10 \AA for Akn 120 and 3C 390.3. At these resolutions, the structure in Akn 120 and 3C 390.3 is just resolved—details at $\sim 250 \text{ km s}^{-1}$ would not be resolved at all. If structure exists in type 1 Seyfert galaxy emission lines on such scales, it has not been probed adequately enough to be revealed.

The unusual features seen in the echelle spectra require high resolution observations to be resolved. Even at a resolution of 1 \AA , the features seen in the echelle data become unremarkable. This is demonstrated in Figure 8.5, which shows the top three echelle orders of the three QSOs smoothed to 1 \AA FWHM resolution and rebinned to 0.4 \AA bins (thus sampling at 2.5 bins per resolution element). Several QSO spectra have been observed at $\sim 1 \text{ \AA}$ resolution, but only a handful at the $\sim 0.1 \text{ \AA}$ of the echelle spectra presented here. It is not surprising, then, that the possible structures noted here have not been noticed before.

Since the BLR is known to be composed of discrete clouds with individual thermal velocity dispersions of $\sim 10 \text{ km s}^{-1}$, the broad emission lines are necessarily composed of the blended emission profiles of many such clouds. Capriotti *et al.* (1981) deduced the number of clouds in type 1 Seyfert galaxy BLRs must be $\gtrsim 10^4$ by comparing emission line data of several galaxies with simulations at resolutions of 5 \AA and 1 \AA . Atwood *et al.* (1982) produced a similar figure of $\gtrsim 5 \times 10^4$ by cross-correlating the H α and H β lines of the type 1 Seyfert galaxy Markarian 509 and searching for significant structures in common. No work has been done on this topic with data of resolution $\sim 0.1 \text{ \AA}$, like those used here. The number of BLR clouds at high relative velocities, producing the extreme wings of the broad emission profile, is much smaller than the total number of clouds—1% of the total or fewer for the spectral regions considered here. This would mean of the order of 10–100 clouds if the total is $\sim 5 \times 10^4$, and the structure caused by the overlapping of their individual profiles would be detectable at 0.1 \AA resolution.

When considering the idea that the features illustrated in Figure 8.2 are caused by structured emission, rather than absorption of a smoothly varying continuum, it

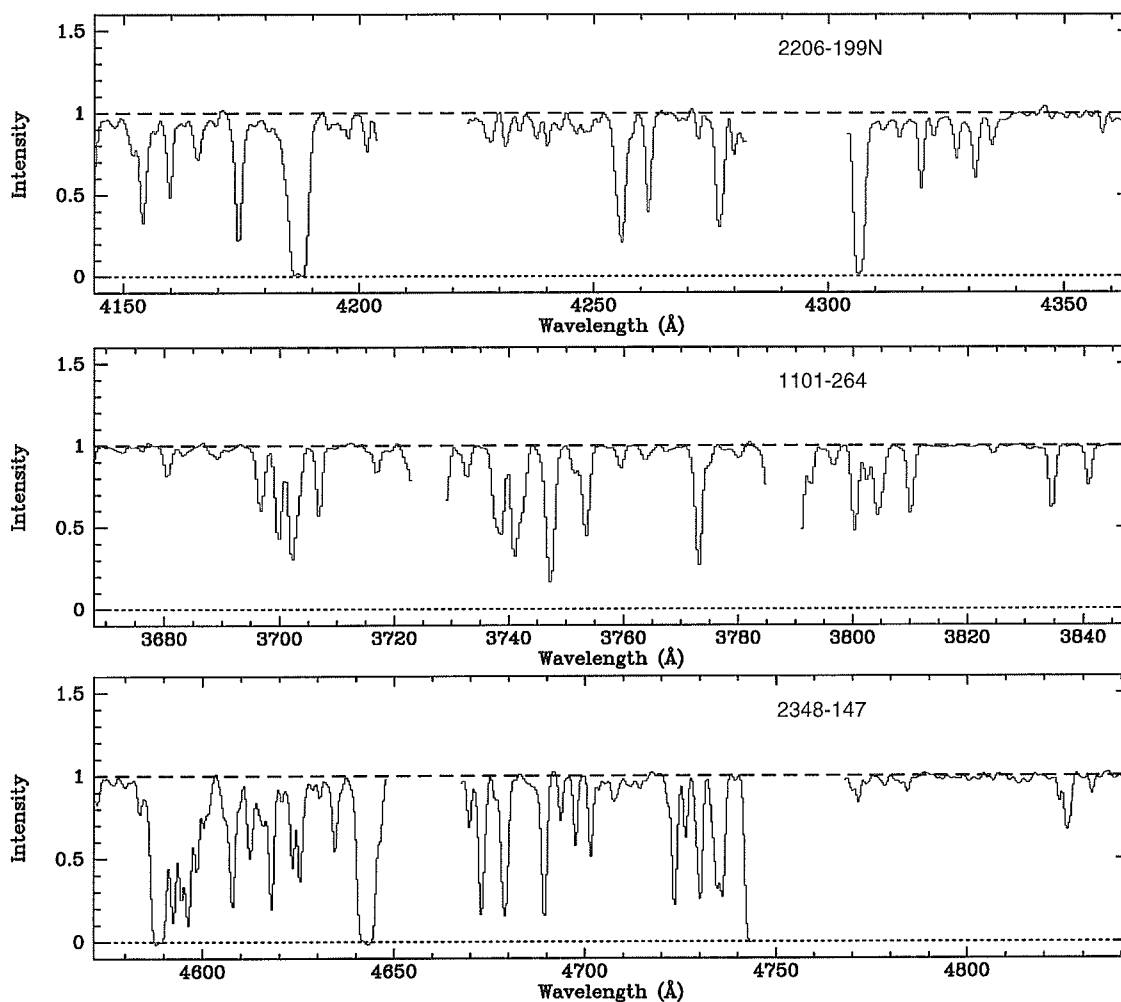


Figure 8.5 The top three echelle orders of Q2206–199N, Q1101–264, and Q2348–147 smoothed to 1 \AA resolution to show how the features shown in Figure 8.2 appear at intermediate resolution. The unusual areas are no longer distinctive and would not be noticed in observations of this resolution.

is important to note that the normalised spectra have already had some structure removed from them. The fitting of a continuum is designed to remove any emission features. The result is a spectrum in which the highest intensity regions all appear close to unit normalised intensity. It may be better to examine the unnormalised spectrum, or to look at a spectrum normalised under the extreme assumption that much of the structure is due to emission. An example of this is shown in Figure 8.6. Given the normalisation shown in Figure 8.6, one could easily believe the structure is caused mostly by a group of emission features covering $\sim 2\text{--}5 \text{ \AA}$ each. While this is in no way a proof that the features are caused by emission, it demonstrates the possibility.

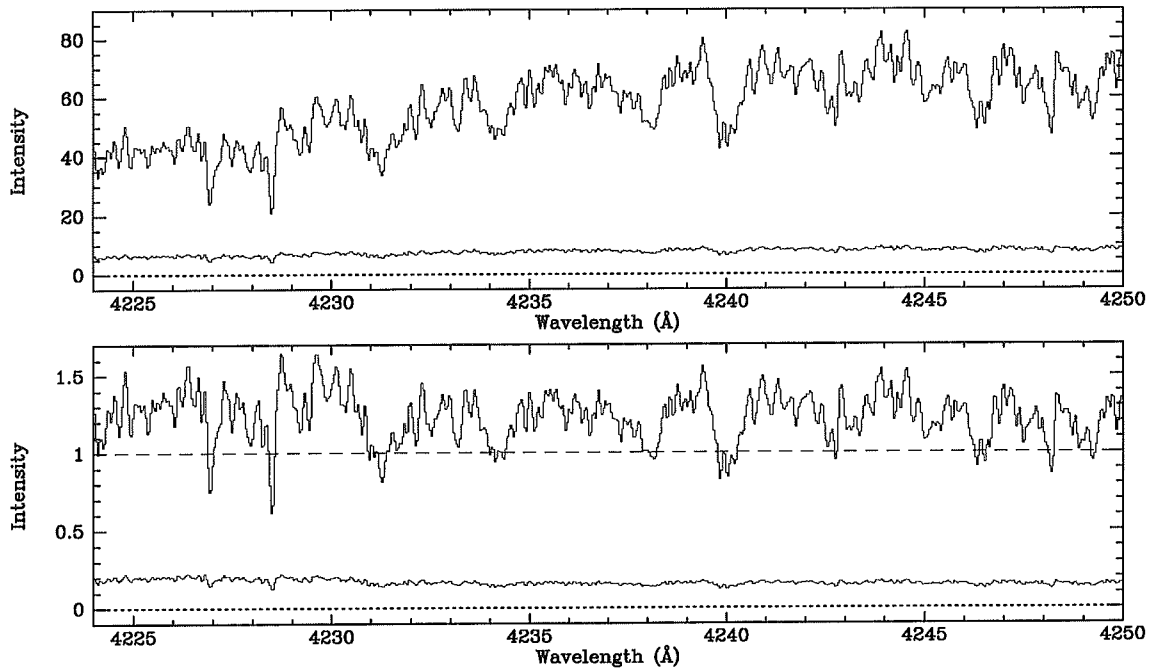


Figure 8.6 A section of the echelle spectrum of Q2206–199N, the same section as shown in the second top panel of Figure 8.2. The noise level is shown in each panel as the jagged line near zero intensity. *Top:* The unnormalised data, showing the unusual structure discussed in Section 8.1. *Bottom:* Hypothetical normalisation, stressing the possibility of most of the structure being due to emission.

8.1.4 Testing the Hypotheses

With three possible explanations for the features observed in the Lyman α emission line wings of the QSOs being studied, it is important to consider how these hypotheses might be tested.

The possibility that the unusual features are a random effect of noise or of blended Lyman α absorption lines can be tested in several ways. An increased S/N ratio is obviously desirable, being the simplest way to minimise the effects of noise and assess the reality of the features. Increasing the sample of objects is another method, since the fraction of those in which similar features are observed becomes statistically significant with a large sample.

To test whether the features are caused by intervening Lyman α absorption, the wings of a different broad emission line, such as C IV $\lambda\lambda 1548, 1550$, could be observed at high resolution and S/N ratio. If the features are caused by such clouds, there would be no detectable C IV absorption (since Lyman α clouds have a very low metal content) and the emission line would have a relatively smooth profile. If, however, the C IV line showed unusual features like those seen in the Lyman α emission line, it would support the arguments that the structures are intrinsic to the QSOs.

One could also observe the red wing of the Lyman α emission line at high resolu-

tion. If this wing shows similar features, then it would be difficult to attribute them to Lyman α absorption and the presence of detectable structure in the emission line would be strongly supported.

The different causes of intrinsic structure would be more difficult to distinguish. The systematic difference in the position of the structure relative to the emission line peak (described in Section 8.1.2) may be observable with good quality data for both wings of a broad emission line. If, on the other hand, no systematic differences can be detected, this would provide evidence in favour of the structure being caused by discrete emission clouds. It is also possible that both mechanisms operate to some degree, in which case careful interpretation of the results of any such observations would be required.

Unfortunately, since the data presented here were taken with the intent of studying the Lyman α forest, the red wing of the Lyman α emission line was not covered. The presence of the N V $\lambda\lambda$ 1238, 1242 Å emission line would complicate any analysis of the red wing of Lyman α emission, but it is to be hoped that future observations will overcome this difficulty and decide whether the features can be attributed to the low S/N ratio of the present data, or are due to absorption or emission. In the latter two cases, such observations could also supply important new constraints on models of the BLR of QSOs. In particular, simulations of ensembles of BLR clouds could be compared with the structures seen in these data, and perhaps both lower and upper limits on the number of BLR clouds in QSO BLRs could be determined.

8.2 Differences Between QSO Sightlines

One of the basic assumptions used by researchers studying the absorption spectra of QSOs is that the QSO sightlines sample representative regions of high- z space. Using this assumption, the characteristics of a small number of QSO sightlines, or even one, have been extrapolated to produce a picture of the Lyman α cloud population in general. With the high resolution observations of different objects presented here, and those published by other researchers, the validity of this assumption can be investigated.

If each individual sightline adequately sampled the Lyman α cloud population, then the following statements would be expected to hold when comparing different sightlines:

1. The number of Lyman α lines with $\log N$ above some chosen completeness limit per unit redshift would be constant at a given redshift, for any QSO spectrum.
2. The column density and velocity dispersion distributions (or equivalent width distribution) of Lyman α lines would be constant for samples at a given redshift.
3. The derived clustering properties of the Lyman α clouds would be similar between sightlines.

Table 8.2 A comparison of the properties of different QSO sightlines.

Object	z_{abs}	$d\mathcal{N}/dz^1$	Median b / km s^{-1}	
			₂	₃
Q1101–264	1.8–2.1	87 ± 16	23^4	32.9^6
Q2206–199N	2.1–2.6	46 ± 10	17^5	26.4^7
Q2348–147	2.1–2.9	213 ± 16	23^4	—
Q0014+813 ⁸	2.3–3.4	287 ± 22	—	33
PKS 2126–158 ⁹	2.9–3.3	187 ± 22	—	26
Q0055–269 ¹⁰	2.9–3.7	251 ± 19	—	26

Notes:

¹ Number of Lyman α lines with $\log N \geq 13.3$ per unit redshift. The uncertainties are 1σ calculated from Poissonian statistics.

² Interactive profile fitting.

³ Automated profile fitting.

⁴ This work.

⁵ Pettini *et al.* (1990) (PHSM).

⁶ Carswell *et al.* (1991) (CLPW).

⁷ Rauch *et al.* (1993).

⁸ Rauch *et al.* (1992).

⁹ Giallongo *et al.* (1993).

¹⁰ Cristiani *et al.* (1995).

In fact, there is evidence that none of these statements is true.

A comparison between the sightlines studied in this thesis and reported in the literature is shown in Table 8.2. A uniform completeness limit of $\log N \geq 13.3$ was imposed on all of the data compiled for the $d\mathcal{N}/dz^1$ values. This was equal to or above the completeness limit specified in each individual study.

As can be seen from Table 8.2, there are significant differences between the number of Lyman α lines per unit redshift between sightlines covering similar redshift intervals. In particular, the sightlines to Q2206–199N and Q2348–147, which cover almost the same redshift interval, show a $> 10\sigma$ difference in line density.

The median b values also show differences between the sightlines. Rauch *et al.* (1993) performed an analysis of the b distributions of the Lyman α lines in the spectra of Q1101–264 (Carswell *et al.*, 1991) and Q2206–199N. A Mann-Whitney test gave a probability of only 0.003 that the two samples were drawn from a b distribution with the same median value. With the median b value (derived from automated line fitting techniques) for Q0014+813 greater than that for Q1101–264 and the median b value for PKS 2126–158 and Q0055–269 less than that for Q2206–199N, there are likely to be even more significant differences in the velocity dispersion distributions.

As discussed in Chapter 7, the clustering properties of the Lyman α clouds along the sightlines to Q1101–264 and Q2348–147 are markedly different.

Other evidence for large differences between sightlines includes the calculations of the Lyman α cloud number density evolution parameter γ presented in Table 6.4 and discussed in Section 6.3.2.

When all of the evidence presented here is accumulated, it seems clear that one cannot rely on a single QSO sightline, or even a small collection of them, to reveal the overall properties of the Lyman α clouds. There are large differences between the properties derived from individual sightlines, even at the same redshifts. In order to gain an overall impression of the properties of the Lyman α clouds, it is necessary to study several sightlines. The total number of sightlines observed at high spectral resolution to date is small, so there is much yet to be learnt by accumulating a larger sample—preferably until several tens of QSOs have been observed at similar resolutions.

In the meantime, the fact that individual QSO sightlines are not representative of the high-redshift universe as a whole must be borne in mind when analysing the properties of the Lyman α clouds.

8.3 Metal Searches in Lyman α Systems

The metal content of the Lyman α clouds has been a subject of concerted research since Sargent *et al.* (1980) (SYBT) first postulated that such objects may be composed entirely of primordial matter, unenriched with metals since the epoch of primordial nucleosynthesis. SYBT showed that clouds with Lyman α rest equivalent width $W_0 \lesssim 1 \text{ \AA}$ had no discernible metal absorption lines, to the limits of their survey.

Based on a study of the QSOs 4C 05.34⁵ ($z_{\text{em}} = 2.877$) and OQ 172⁶ ($z_{\text{em}} = 3.544$), Norris *et al.* (1983) were the first to claim a detection of an associated heavy element line in Lyman α systems with $W_0 < 1 \text{ \AA}$. They used a method in which the spectra were shifted to the rest frame of each Lyman α system with $W_0 \geq 460 \text{ m\AA}$, then summed to produce a composite which was searched for metal lines at the appropriate (rest) wavelengths. In this way, they detected a feature at the wavelengths of O VI $\lambda\lambda 1031, 1037$ (the lines of the doublet were added to increase S/N), which they concluded had a 96% probability of being real. Measuring the equivalent width and applying curve-of-growth analysis and a reasonable photoionisation model of the Lyman α clouds, they produced a best estimate for the logarithmic abundance of oxygen relative to solar of $[\text{O}/\text{H}] = -1.9$ at a mean redshift $\langle z_{\text{abs}} \rangle = 2.9$. This is typical of oxygen abundances in Population II material and implies the Lyman α cloud material is not primordial in composition. However, Williger *et al.* (1989) failed to detect O VI in a similar study of four QSOs at higher sensitivity and concluded that Norris *et al.*'s detection was likely due to chance.

Another approach to determining the metal content of Lyman α clouds is to search for metal lines associated with individual clouds of high $N(\text{H I})$. Chaffee *et*

⁵4C 05.34 is also known as Q0805+046.

⁶OQ 172 is also known as Q1442+101.

al. (1986) (hereafter CFBW) produced an upper limit of $[C/H] \leq -3.5$ based on a search for C III $\lambda 977$ in two Lyman α clouds of $\log N(\text{H I}) = 16.3, 16.7$ at $z_{\text{abs}} = 3.3$ ⁷.

Using the co-addition method with a sample of 14 QSOs, Lu (1991) reported a detection of C IV $\lambda \lambda 1548, 1550$ at $\langle z_{\text{abs}} \rangle = 2.5$ at $\geq 99.99\%$ significance. This implied $[C/H] = -3.2$ for Lyman α clouds of $400 \leq W_0 \leq 800 \text{ m\AA}$ (on the saturated part of the curve-of-growth, so with ill-defined $N(\text{H I}) \gtrsim 10^{14} \text{ cm}^{-2}$). The inconsistency with CFBW is, as noted by Lu, probably due either to observational uncertainty or to the fact that the relatively high $N(\text{H I})$ clouds used by CFBW may not be representative of the metallicity and ionisation conditions of the majority of weaker Lyman α clouds.

Tytler and Fan (1994) used the co-addition method on a 10 km s^{-1} resolution spectrum of HS 1946+7658 and failed to detect any C IV absorption at the 2σ level in a sample of 65 Lyman α clouds with mean $N(\text{H I}) = 1.0 \times 10^{14} \text{ cm}^{-2}$ and $\langle z_{\text{abs}} \rangle = 2.8$. The lines detected by Lu were 5 times stronger than Tytler and Fan's upper limit, but Tytler and Fan point out that their sample had a mean $N(\text{H I}) \sim 25$ times lower than Lu's. They argued Lu's sample was more likely to contain Lyman α systems with weak C IV absorption than their own because of this difference in $N(\text{H I})$ and so the results were compatible. This was demonstrated when they calculated their metallicity upper limit to be $[C/H] \leq -2.0$. They concluded that easily detectable C IV was restricted to high $N(\text{H I})$ clouds, and that new instruments such as the *Hubble Space Telescope* and 10 m Keck Telescope would be required to detect metals in typical Lyman α forest clouds⁸.

Although the co-addition of Lyman α systems allows sensitive searches for metals to be made, there is the possibility that the sample will be contaminated by a small population of relatively metal-rich objects. Given this, positive detections such as Lu's need to be treated with caution. Using very high S/N and resolution spectra from the Keck Telescope, Cowie *et al.* (1995) examined individual Lyman α systems with $N(\text{H I}) \geq 3 \times 10^{14} \text{ cm}^{-2}$ (*i.e.* saturated lines) at $\langle z_{\text{abs}} \rangle \simeq 2.6$ to determine what fraction of such clouds had detectable C IV absorption. Measurable C IV was detected in 15 of 31 systems, giving a mean $[C/H] = -2.7$ (using the same ionisation model as Lu). Cowie *et al.* also co-added their data for Lyman α systems with $N(\text{H I}) < 3 \times 10^{14} \text{ cm}^{-2}$, deriving a 2σ upper limit of $[C/H] \leq -2.5$ for these clouds, with a mean $N(\text{H I}) = 7 \times 10^{13} \text{ cm}^{-2}$, again in agreement with Lu and Tytler and Fan.

Using the same data, Cowie *et al.* measured C II $\lambda 1334$ and N V $\lambda 1238$ lines in a sample of the strong Lyman-limit systems (LLS). They concluded $[C/H] \sim [N/H] \sim -2$ in the LLS clouds. Then, comparing the LLS results with those for lower $N(\text{H I})$ systems, they concluded the simple ionisation model used by Lu needed

⁷An earlier paper, Chaffee *et al.* (1985), claimed a tentative detection of Si III $\lambda 1206$ for these clouds, implying $[Si/H] = -2.7$, but after the C III measurement CFBW concluded the Si III detection was not real.

⁸Note added in revision: Tytler *et al.* (1995) reported in a study of two QSOs with data from the Keck Telescope that 60% of Lyman α clouds with $\log N(\text{H I}) > 14.5$ contained detectable C IV absorption, implying $[C/H] > -2.5$ in about 50% of the clouds.

to be modified to reflect a higher ionisation of the weaker systems. Given this change to the ionisation model, the limits on the C IV measurements for the lower $N(\text{H I})$ systems become consistent with $[\text{C}/\text{H}] \sim -2$, which Cowie *et al.* claim is typical of all Lyman α systems with $N(\text{H I}) \geq 10^{14} \text{ cm}^{-2}$. They proposed self-heating by star formation as the mechanism for producing these metallicities and high ionisations.

Recently Lanzetta *et al.* (1995) imaged fields around HST spectroscopic target QSOs to search for galaxies at the redshifts of absorption systems in the QSO sightlines. They presented evidence that many, if not most, of the Lyman α clouds at $z_{\text{abs}} \leq 1$ are associated with the extended envelopes of luminous galaxies. If this trend is followed at higher z_{abs} , then some metal enrichment of the Lyman α clouds might be expected. The limits and detections claimed in the literature are so far consistent with this picture. There may still be a population of primordial clouds, but the evidence for metal enrichment in at least a subset of the Lyman α clouds with $N(\text{H I}) \geq 10^{14} \text{ cm}^{-2}$ is now strong.

8.3.1 Looking for Metals in Q1101–264 and Q2348–147

Although the AAT UCLES data for Q1101–264 and Q2348–147 are not of high enough S/N to allow detection of individual metal lines associated with Lyman α clouds, it is still possible to use the co-addition technique to search for metals and come to some conclusions on the cloud metallicities. These spectra, particularly those of Q1101–264, allow clouds of relatively low $N(\text{H I})$ to be examined because of the very high resolution.

Subsets of the Lyman α systems in each object were examined to see if there were any detectable metal lines in Lyman α systems in these two objects, or to determine upper limits to metal abundances if none were detected.

Generating Composite Spectra

In each case, Lyman α lines with fitted column densities above a certain cut-off (different for each object) were selected, since these would be the major contributors to a detectable metal line, making the reasonable assumption that the weakest Lyman α systems would not be the most metal-rich. In fact, Lu (1991) has pointed out that, under reasonable assumptions, adding lines below a certain cut-off in column density *degrades* the metal line signals being searched for, because of the additional noise in the absorption feature. Unfortunately, the optimal column density cut-off for such a search cannot be calculated without knowing the distribution of metallicity and ionisation levels as a function of $N(\text{H I})$.

For Q1101–264, Lyman α systems with fitted $N(\text{H I}) \geq 10^{13} \text{ cm}^{-2}$ were selected, and for Q2348–147, systems with $N(\text{H I}) \geq 10^{14} \text{ cm}^{-2}$ were chosen. The reason for the different choice is that the two objects have a very different distribution of neutral hydrogen column density. In Q1101–264 there is only a handful of systems with $N(\text{H I}) \geq 10^{14} \text{ cm}^{-2}$, whereas in Q2348–147 there are 48. With so many systems of high column density along the sightline to the latter object, the contribution from

systems with $N(\text{H I}) \leq 10^{14} \text{ cm}^{-2}$ is negligible, whereas such systems comprise the majority of the total H I column density on the sightline to the former. Using the lower cut-off for Q1101–264, 48 Lyman α systems were selected, the same number as selected for Q2348–147. For Q2348–147 the median value of $\log N(\text{H I})$ is 14.45, while for Q1101–264 it is $\log N(\text{H I}) = 13.40$.

The spectral regions corresponding to a set of metal lines at the Lyman α redshifts were then co-added in rest frame wavelengths. The metal lines selected for investigation were chosen to be strong lines close in wavelength to $\lambda_{\text{Ly}\alpha} = 1215.67 \text{ \AA}$ so the wavelength coverage of the spectra would allow a significant number of regions to be co-added. The lines chosen were C I $\lambda 1277$, C II $\lambda 1334$, N V $\lambda 1238$, O I $\lambda 1302$, Si II $\lambda 1193$ and $\lambda 1260$, and Si III $\lambda 1206$. The lines of C II and Si III are particularly suited for a search because they are strong lines and the ionisation stages are predominant over a wide range of ionisation levels (or temperatures). The N V $\lambda 1242$ and Si II $\lambda 1190$ doublet members were not examined, as these lines have λf values about half those of their doublet partners, making the possibility of detection smaller. Only spectral regions which were not obviously contaminated by the presence of other, detected, absorption lines were included in the summation. In general, this criterion resulted in about half of the 48 spectral regions being rejected for each QSO. Other regions could not be included in the sum because they fell outside the wavelength coverage of the spectrum, or in inter-order gaps.

For each composite spectrum, the mean value of $\log N(\text{H I})$ was calculated, as well as the median value. The mean of $\log N(\text{H I})$, which is the logarithm of the geometric mean of $N(\text{H I})$, is a more robust estimator of the population mean than the arithmetic mean of $\log N(\text{H I})$ when the data span several orders of magnitude, as they do in this case. In each case the mean-log is consistent with the median to within standard error estimates, whereas the arithmetic mean is often not. For the abundance calculations, the mean-log values were used.

Calculating Abundance Limits

After generation of the composite spectra, attempts were made to fit absorption profiles at the expected metal line wavelengths. Such fits are meaningful because the co-addition of spectral regions and subsequent renormalisation produces the mean of any line equivalent widths, and any lines present are expected to be weak and hence lie on the linear part of the curve-of-growth, so the column densities will also add linearly. In no case was an obvious absorption line present in the co-added data at the expected wavelength, so the attempted fits give only upper limits for the metal column densities. The mean $N(\text{H I})$ of the corresponding Lyman α lines in each case was also calculated from the values given by profile fitting.

The attempted metal profile fits were made with assumed b values differing under the following assumptions:

1. Purely thermal broadening: When the velocity dispersion of the H I and the

metal is due only to thermal motion, the metal line b value is given by

$$b_{\text{metal}} = \sqrt{\frac{m_{\text{H}}}{m_{\text{metal}}}} b_{\text{Ly}\alpha}, \quad (8.1)$$

where m_{H} and m_{metal} are the atomic masses of hydrogen and the metal ion respectively.

2. Fully turbulent broadening: In this case, the bulk motions affect both the H I and the metal identically, so

$$b_{\text{metal}} = b_{\text{Ly}\alpha}. \quad (8.2)$$

These two assumptions are the extremes of a possible range of b values. In general, the metal line velocity dispersion will be composed of thermal and turbulent components, and so will fall between the two extremes. For each QSO, $b_{\text{Ly}\alpha}$ was chosen to be the mean b of the 48 selected lines greater than the relevant $N(\text{H I})$ cut-off. These were $b_{\text{Ly}\alpha} = 26 \text{ km s}^{-1}$ for Q1101–264 and $b_{\text{Ly}\alpha} = 35 \text{ km s}^{-1}$ for Q2348–147. Fits were then attempted with b_{metal} values given by Equations 8.1 and 8.2.

To derive abundance limits from the metal ion column density limits, the quantitative photoionisation model presented by CFBW was used. CFBW adopted the qualitative model proposed by SYBT and used Ferland’s CLOUDY photoionisation code (Ferland and Netzer, 1983) to produce a set of curves showing the column densities of various metal ions as a function of total hydrogen density in a cloud with $\log N(\text{H I}) = 16.5$ and the logarithmic metal-to-hydrogen ratio relative to the solar value $[Z/\text{H}] = -1.7$ (their Figure 1). The radiation field used was detailed in Bechtold *et al.* (1987)⁹ and was corrected for absorption by Lyman α forest and optically thick Lyman α disc systems. This field assumes all ionising radiation is produced by background QSOs with the luminosity function of Schmidt and Green (1983). The adopted logarithmic solar abundances with respect to hydrogen for the elements investigated here were those used by CFBW. The abundances and the oscillator strengths used (Morton *et al.*, 1988) are summarised in Table 8.3.

The derived upper limits on the column densities of the measured metal ions and the corresponding mean $N(\text{H I})$ values were converted into logarithmic abundances relative to the solar values shown in Table 8.3. This was done for two different levels of ionisation, towards opposite ends of CFBW’s “allowable range” of ionisations at $z = 2$ (calculated using upper and lower Lyman α cloud size limits from Sargent *et al.* (1982) and Foltz *et al.* (1984) respectively). The ionisation levels chosen corresponded to hydrogen neutral fractions $n(\text{H I})/n(\text{H}) = 10^{-4}$ and 10^{-3} .

8.3.2 Metal Search Results

The composite spectra for the investigated metal lines are shown for Q1101–264 in Figure 8.7 and for Q2348–147 in Figure 8.8. The details of the derived ion

⁹This paper details several different radiation fields, parametrised by various descriptive terms. The field used by CFBW is described as the SG case HL1, no-cut, “medium” field.

Table 8.3 Relative solar logarithmic abundances of elements searched for in Lyman α systems and oscillator strengths of the transitions.

Element	Ionisation	λ_0 Å	Logarithmic abundance	f
H	I	1215.6701	0.00	0.4162
C	I	1277.2454	-3.33	0.0881
C	II	1334.5323	-3.33	0.118
N	V	1238.821	-4.01	0.152
O	I	1302.1685	-3.08	0.0486
Si	II	1193.2898	-4.40	0.501
Si	II	1260.4223	-4.40	0.959
Si	III	1206.500	-4.40	1.66

column density and element abundance upper limits for the two objects are shown in Table 8.4 (Q1101–264) and Table 8.5 (Q2348–147).

A summary of the abundance limits and a comparison with published values is shown in Table 8.6.

It should be noted that the composite spectral regions shown in Figures 8.7 and 8.8 may have their continuum levels depressed by the “smearing” of several weak Lyman α lines. Since no obvious absorption lines were present at the expected metal line positions, it is likely that much of the depression measured in calculating the upper limits of metal ion column densities is caused by such Lyman α absorption. After all, it would be a remarkable coincidence if the integrated Lyman α absorption left absorption “holes” precisely where the metal lines are expected, and which were filled by the metal absorption. This means that the upper limits quoted on element abundances are fairly conservative.

In the high-ionisation model, the low-ionisation species investigated (C I, O I, Si II, and Si III) unfortunately do not provide any useful limits on elemental abundances because these ions comprise negligible fractions of the total amount of each element present in the chosen model. The limits for carbon and nitrogen derived from C II and N V are more useful. A similar situation also occurs in the low-ionisation model, except that Si III is now the dominant ion-stage of silicon and provides a measurable limit.

In each object, the low-ionisation model silicon limits are not very restrictive. The only previous measurement of silicon abundance in QSO spectra (Chaffee *et al.* (1985)) was a tentative detection implying $[\text{Si}/\text{H}] = -2.7$. This is well below the limits measured here, and the detection was later concluded not to be real by CFBW, making it also only an upper limit.

The high-ionisation model carbon limits are consistent with those obtained by Lu (1991) and Tytler and Fan (1994). Although they do not provide stronger limits, it is important to note that the Q1101–264 measurement of $[\text{C}/\text{H}] \leq -0.7 \pm 0.1$ (assuming fully thermal Doppler widths) is for a set of lines significantly weaker

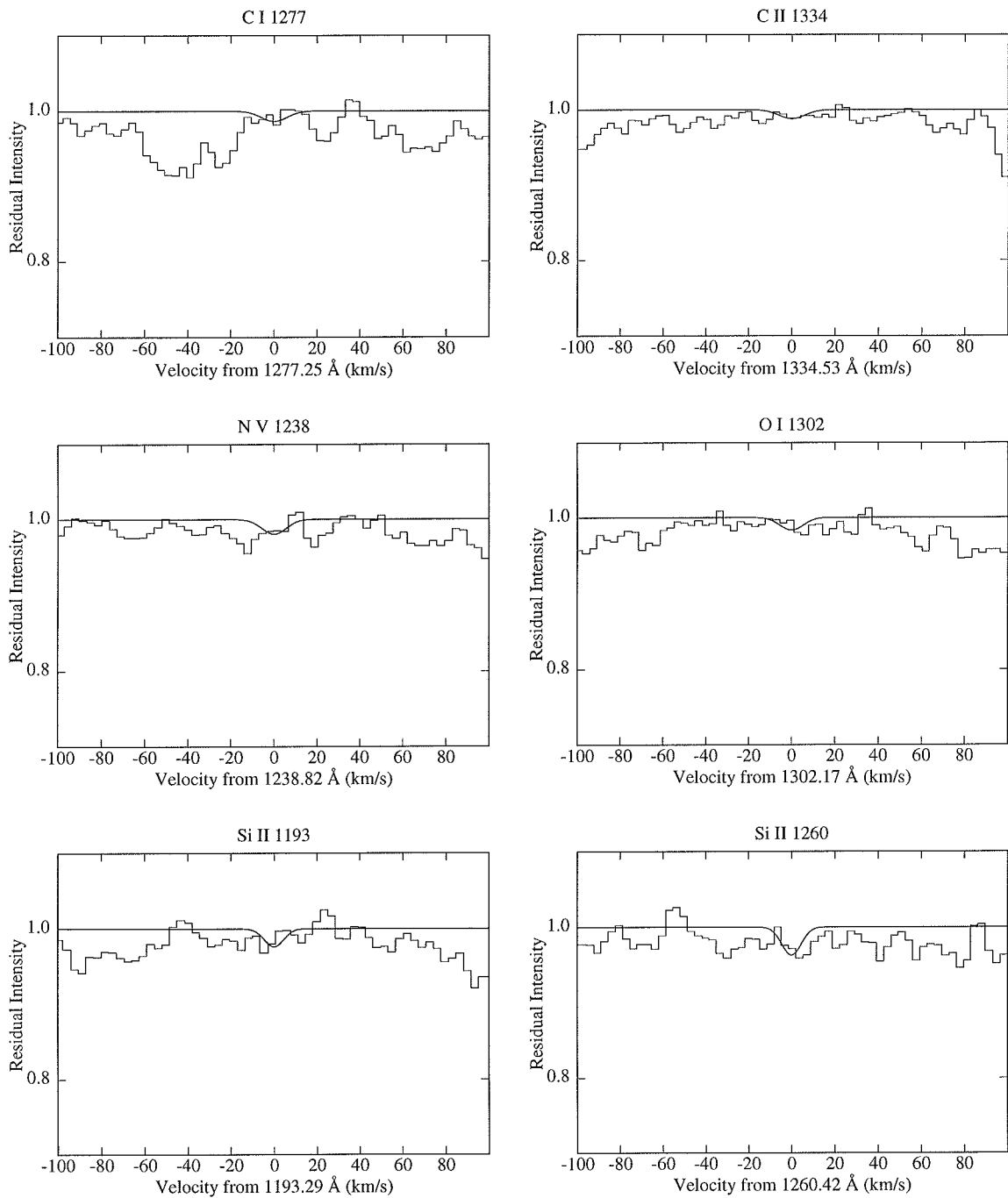


Figure 8.7 Profile fits to composite spectra at the expected positions of various metal lines in Lyman α systems in Q1101–264. These are the best fits for the smallest b values given for each element in Table 8.4.

Table 8.4 Profile fit parameters and upper limits to element abundances for composite spectra of Lyman α systems in Q1101–264. Uncertainties are formally 1σ , but see the text in Section 8.3.2.

Ion	λ_0 Å	\mathcal{N} ¹	log $N(\text{H I})$		b_{metal} kms ⁻¹	log N_{metal} ²	[X/H] ³	
			mean log	median			high ⁴	low ⁵
C I	1277.2454	14	13.3 ± 0.1	13.3 ± 0.1	7.5	11.8 ± 0.1	—	—
					26.0	12.2 ± 0.2	—	—
C II	1334.5323	10	13.4 ± 0.1	13.5 ± 0.1	7.5	11.6 ± 0.1	-0.7 ± 0.1	-1.2 ± 0.1
					26.0	12.0 ± 0.1	-0.3 ± 0.1	-0.8 ± 0.1
N V	1238.821	28	13.5 ± 0.1	13.4 ± 0.1	6.9	11.7 ± 0.1	-1.7 ± 0.1	-1.0 ± 0.1
					26.0	12.3 ± 0.2	-1.1 ± 0.2	-0.4 ± 0.2
O I	1302.1685	13	13.5 ± 0.1	13.5 ± 0.1	6.5	12.1 ± 0.1	—	—
					26.0	12.6 ± 0.2	—	—
Si II	1193.2898	25	13.5 ± 0.1	13.5 ± 0.1	4.9	11.2 ± 0.1	—	—
					26.0	11.4 ± 0.2	—	—
Si II	1260.4223	14	13.5 ± 0.1	13.5 ± 0.1	4.9	11.1 ± 0.1	—	—
					26.0	11.6 ± 0.2	—	—
Si III	1206.500	22	13.5 ± 0.1	13.5 ± 0.1	4.9	10.9 ± 0.1	—	-0.3 ± 0.1
					26.0	11.2 ± 0.2	—	-0.0 ± 0.2

Notes:

¹ \mathcal{N} is the number of spectral regions co-added.

² Upper limit.

³ Upper limit for the logarithmic abundance of the given element (“X”) relative to solar.

A dash indicates an upper limit > 0.0 , *i.e.* greater than solar abundance.

⁴ High ionisation case; $n(\text{H I})/n(\text{H}) = 10^{-4}$.

⁵ Low ionisation case; $n(\text{H I})/n(\text{H}) = 10^{-3}$.

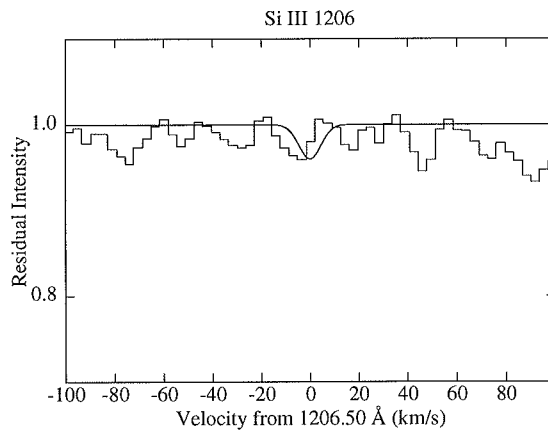


Figure 8.7 *Continued.*

Table 8.5 Profile fit parameters and upper limits to element abundances for composite spectra of Lyman α systems in Q2348–147. Uncertainties are formally 1σ , but see the text in Section 8.3.2.

Ion	λ_0 Å	\mathcal{N} ¹	$\log N(\text{H I})$		b_{metal} km s^{-1}	$\log N_{\text{metal}}$ ²	$[\text{X}/\text{H}]^3$	
			mean log	median			high ⁴	low ⁵
C I	1277.2454	17	14.6 ± 0.2	14.6 ± 0.3	10.1	12.7 ± 0.1	—	—
					35.0	13.1 ± 0.2	—	—
C II	1334.5323	10	14.9 ± 0.2	14.8 ± 0.2	10.1	12.3 ± 0.1	-1.5 ± 0.2	-2.0 ± 0.2
					35.0	12.9 ± 0.2	-0.9 ± 0.3	-1.4 ± 0.3
N V	1238.821	24	14.5 ± 0.1	14.4 ± 0.1	9.4	12.5 ± 0.1	-1.9 ± 0.1	-1.2 ± 0.1
					35.0	12.9 ± 0.2	-1.5 ± 0.2	-0.8 ± 0.2
O I	1302.1685	14	14.7 ± 0.2	14.4 ± 0.3	8.8	12.6 ± 0.1	—	—
					35.0	13.0 ± 0.2	—	—
Si II	1193.2898	22	14.4 ± 0.1	14.4 ± 0.1	6.6	11.5 ± 0.1	—	—
					35.0	12.3 ± 0.2	—	—
Si II	1260.4223	16	14.7 ± 0.2	14.7 ± 0.2	6.6	11.2 ± 0.1	—	—
					35.0	11.8 ± 0.2	—	—
Si III	1206.500	28	14.6 ± 0.1	14.4 ± 0.2	6.6	11.4 ± 0.1	—	-0.9 ± 0.1
					35.0	12.1 ± 0.2	—	-0.2 ± 0.2

Notes:

¹ \mathcal{N} is the number of spectral regions co-added.

² Upper limit.

³ Upper limit for the logarithmic abundance of the given element (“X”) relative to solar.

A dash indicates an upper limit > 0.0 , *i.e.* greater than solar abundance.

⁴ High ionisation case; $n(\text{H I})/n(\text{H}) = 10^{-4}$.

⁵ Low ionisation case; $n(\text{H I})/n(\text{H}) = 10^{-3}$.

Table 8.6 Summary of metal abundance measurements and published values. For the two QSOs studied in this work, only the high-ionisation model value is given, corresponding to similar ionisation models in the published data. All values are upper limits, except where noted.

Reference	z	[C/H]	[N/H]	[Si/H]
Q1101–264	1.8–2.1	-0.7 ± 0.1	-1.7 ± 0.1	—
Q2348–147	2.1–2.9	-1.5 ± 0.2	-1.9 ± 0.1	—
Chaffee <i>et al.</i> (1985)	3.4	—	—	-2.7
Chaffee <i>et al.</i> (1986)	3.3	-3.5	—	—
Lu (1991)	1.9–3.3	-3.2^1	—	—
Tytler and Fan (1994)	2.5–3.0	-2.0	—	—
Cowie <i>et al.</i> (1995)	2.3–3.0	~ -2	~ -2	—
Tytler <i>et al.</i> (1995)	2.4–3.1	-2.5^1	—	—

Notes:

¹ Detection.

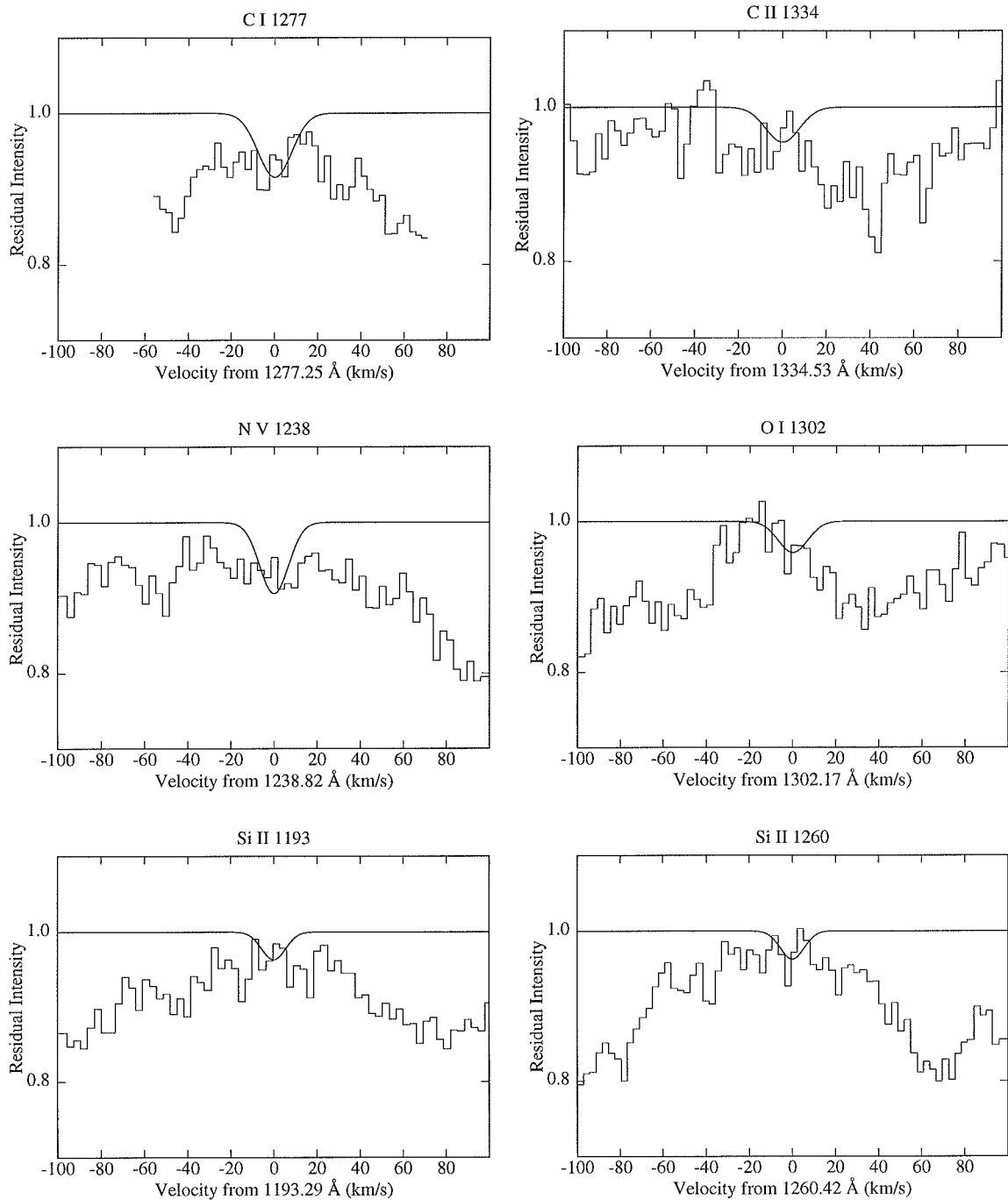
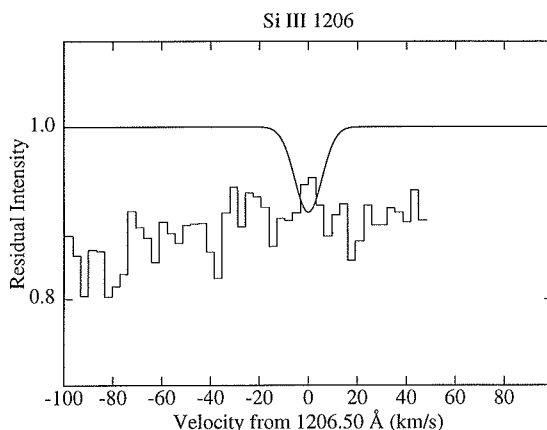


Figure 8.8 Profile fits to composite spectra at the expected positions of various metal lines in Lyman α systems in Q2348–147. These are the best fits for the smallest b values given for each element in Table 8.5.

Figure 8.8 *Continued.*

than those previously measured. If the low-ionisation model is closer to reality than the high-ionisation model, then the carbon abundance limits are significantly lower, but of course still not as strong as those of Lu and Tytler and Fan (because their limits require similar adjustment for the ionisation model).

The nitrogen limits are perhaps the most interesting. The Q1101–264 result of $[N/H] \leq -1.7 \pm 0.1$ and the value $[N/H] \leq -1.9 \pm 1.0$ from Q2348–147 (high-ionisation model) are consistent with the value claimed by Cowie *et al.* (1995) in LLS clouds, but do not improve on that result. These limits are just compatible with the possibility that Lyman α clouds as weak as $N(\text{H I}) = 10^{13} \text{ cm}^{-2}$ share the metallicity $[N/H] \sim -2$ proposed by Cowie *et al.* for clouds with $N(\text{H I}) = 10^{14}$. If the low-ionisation model applies, the limits are considerably less restrictive.

Which ionisation model is closer to reality is unclear, but Tytler and Fan and Cowie *et al.* point out that higher ionisations are likely at lower neutral hydrogen column densities. If the relatively low $N(\text{H I})$ clouds studied here are indeed more highly ionised than those of previous samples, the limits set here for nitrogen may be slightly stronger because NV should then be more easily detectable, but the carbon and silicon limits will be even weaker. In the unlikely low-ionisation case, the nitrogen limits are considerably less restrictive. Furthermore, the results for Q1101–264 are at a significantly lower redshift than those for Q2348–147 and all of the published results. CFBW point out that the ionisation of the Lyman α clouds will increase with decreasing z , assuming they are in pressure equilibrium with an adiabatically evolving medium. This may make the $[N/H]$ limits for Q1101–264 somewhat stronger relative to those for Q2348–147, but probably still not as strong, and further degrade the usefulness of the Q1101–264 $[C/H]$ limits.

An additional complication in the case of nitrogen comes from the result by Pettini *et al.* (1995) that nitrogen is under-abundant relative to other elements in a $z_{\text{abs}} = 2.28$ galaxy. The galaxy is a damped Lyman α absorber along the sightline to Q2348–147. Their measurement of the nitrogen to oxygen (N/O) ratio showed that, relative to solar abundance, nitrogen was at least 15 times more under-abundant

than oxygen. This demonstrated that nitrogen production at high redshifts is delayed substantially compared with other elements, as described theoretically by the nucleosynthesis models of Vila-Costas and Edmunds (1993). If the Lyman α clouds also have such N/O ratios, as would seem likely, then it is not surprising that no nitrogen detections have yet been claimed, and the limits presented here would not even approach the expected nitrogen abundances.

The search for metal lines in Lyman α systems and the subsequent abundance measurements are difficult procedures, but they promise to provide important constraints on the metal enrichment of the early universe. The work done so far has been inconclusive and the ionisation modelling of the Lyman α clouds needs to be improved before a full understanding is achieved. There are strong hints that some of the Lyman α clouds could contain metals in quantities similar to that of Population II stellar material, but the existence of some truly primordial clouds with $N(\text{HI}) \leq 10^{14}$ cannot be ruled out.

Chapter 9

Summary and Further Work

9.1 The Cloudy Night QSO

The analysis of the Cloudy Night QSO (CNQ) spectrum and subsequent comparison of the results with the simulation input parameters showed that interactive data reduction procedures were able, in general, to reproduce the absorption line parameters with uncertainty estimates that approximated 1σ confidence limits. This was despite the systematically low continuum fits which were adopted.

The continuum was fitted interactively in the knowledge that automated fitting procedures invariably place the continuum too low and with the aim of placing it as high as could be justified by the data. Nonetheless, the resulting fits were mostly 5–10% too low, showing that the plethora of absorption features produced an apparent lowering of the continuum which could not adequately be accounted for without the benefit of analysing such a simulation.

No systematic bias was found in the fitted column densities of the absorption lines. This may seem surprising given the fact that the continuum levels were set systematically low. One might expect the line equivalent widths also to be low by 5–10%, giving rise to a systematic error in the column densities. However, the absorption which lowers the apparent continuum is generally composed of numerous weak, blended lines, which also affect the profiles of the stronger lines. The average effect is like a genuine lowering of the continuum level. If the fitted continuum reflects this apparent lower continuum, then the effect is removed in the normalisation and the equivalent widths of strong lines are relatively unaffected. In this sense it may be better to fit what appears to be the continuum level, and not worry about whether or not it is the true continuum level. Of course, it would be better still to characterise and measure the numerous weak lines which produce the apparent continuum lowering, but this has not yet been achieved.

A systematic bias was found for the measured velocity dispersions, with b being underestimated by $1.1 \pm 0.3 \text{ km s}^{-1}$ on average. This bias was found to be correlated with the true b values in the sense that larger b values were more likely to be underestimated by larger amounts, but it was uncorrelated with the measured b values. A

suitable calibration to remove the bias from measurements of real QSOs could not be constructed, since the scatter in the b errors was large and it was not clear that any adjustment would significantly improve the reliability of measurements.

9.1.1 Lyman α Line Distributions

It was determined that the shape of the Lyman α column density distribution could be recovered from the CNQ spectrum, despite the problems of incompleteness at low values of $N(\text{HI})$ caused by limited S/N ratio and the effects of line blending. This is an encouraging result for the analyses of the column density distributions of Lyman α clouds along the sightlines to real QSOs, showing that high resolution spectra are adequate for investigating the $N(\text{HI})$ distribution.

The investigation of the apparent correlation between b and $N(\text{HI})$ in the CNQ data showed that several effects combined to enhance an existing correlation. Contamination of the Lyman α sample by unidentified metal lines introduced a number of low b value lines. A line detection threshold removed lines with low $N(\text{HI})$ and high b from the measured sample. Fitting errors in the line parameters acted to move the positions of lines in the b - $\log N(\text{HI})$ plane. The combined consequence of these three effects was to enhance the significance of the existing correlation b - N correlation and to increase the slope of b versus $\log N$.

It is clear that line selection and fitting biases are prone to induce an apparent correlation between b and $\log N$, as reported by Rauch *et al.* (1993), but it is also the case that a strong measured correlation could still be indicative of an underlying true correlation.

9.1.2 Metal Line Identifications

It was found that there was a contamination rate of $\sim 20\%$ unidentified metal lines in the CNQ Lyman α line sample. This was seen as a high extreme because of the atypically large number of heavy element systems present in the spectrum and the difficulty of identifying them amongst the large number of other lines.

The high number of unidentified metal lines did, however, emphasise that there are many situations in which metal lines can escape identification. Some of these are bound to occur in almost any Lyman α forest spectrum, so the generally assumed “negligible” rate of contamination estimated in published work must be treated with some degree of scepticism.

9.1.3 Future Work on QSO Simulations

The study of the CNQ spectrum has proved to be an invaluable aid in the analysis and interpretation of real QSO spectra. The biases and errors present in the interactive approach to absorption line data reduction have been revealed. It would be equally instructive to examine in detail the results of automated data reduction techniques applied to the same data. This is in fact underway, with Saskia Besier,

John Webb, and Bob Carswell analysing the CNQ data under the same conditions as the present work.

Once the automated analysis of the CNQ spectrum is complete, a detailed comparison of the results with those presented here should reveal the relative advantages and disadvantages of the automated and interactive processes.

Ideally, a large set of different simulations would be analysed in various ways to build up a comprehensive description of the biases present in all of the spectral analysis techniques in use. This is obviously an enormous task, and it is doubtful that any researchers would devote the necessary time to it.

9.2 Metal Line Systems

The metal line systems found in the QSOs 1101–264 and 2348–147 were described in detail.

Six redshift systems in the spectrum of Q1101–264, previously reported by other authors, were seen and their component structures at high resolution were described and compared with the published data. In general, the results were consistent with the previous observations. Two possible new redshift systems were proposed, based on plausible identifications of isolated narrow lines, but there was not enough evidence to establish the systems. One redshift system proposed by Carswell *et al.* (1984), consisting solely of a Mg II $\lambda\lambda 2796, 2803$ doublet at $z_{\text{abs}} = 0.356$, was examined carefully and found to be more consistent with an identification of the lines as single Lyman α lines.

Seven heavy element systems in the spectrum of Q2348–147 were described. One was a damped Lyman α system at $z_{\text{abs}} = 2.279$, which has been analysed in detail by Pettini *et al.* (1995). All of the other systems were seen to contain C IV $\lambda\lambda 1548, 1550$ doublets and very few other lines. In particular, no low ionisation lines (with the exception of saturated Lyman α lines) were seen in any system, despite several such lines being within the spectral coverage. These are therefore high ionisation systems, typical of sightlines through hot galaxy haloes.

9.2.1 Searches for Metals in Lyman α Forest Systems

A search for detectable signs of metal absorption in the Lyman α forest systems of Q1101–264 and Q2348–147 was carried out using the method of co-addition of spectra at the expected wavelengths of metal lines.

No evidence of metal absorption was present in any case. The most interesting upper limit on the metal abundance in the Lyman α clouds was for nitrogen in the Q2348–147 data. Assuming a high-ionisation model with $n(\text{HI})/n(\text{H}) = 10^{-4}$ and a nitrogen ion velocity dispersion of $b = 9 \text{ km s}^{-1}$, the upper limit on the logarithmic nitrogen abundance relative to solar was $[\text{N}/\text{H}] \sim -1.9 \pm 0.1$, similar to the value found by Cowie *et al.* (1995) for Lyman α lines of much greater column density.

It would be of great importance to detect the presence of heavy elements in Lyman α forest systems. If the Lyman α clouds are composed of matter unenriched since the epoch of primordial nucleosynthesis, as first postulated by Sargent *et al.* (1980, SYBT), then they provide unique windows to the composition of the universe at the earliest observable epochs. If metals are commonly detected in Lyman α clouds, it would provide important constraints on the epoch of galaxy formation and metal enrichment of the early universe. With the new class of 8–10 m optical telescopes, the high S/N ratios and number of spectra required to make metal detections, or place extreme limits on the Lyman α cloud metal abundances, should be attainable. Such studies form important work for the future.

9.3 The Column Density Distribution

The distributions of Lyman α cloud column densities in the spectra of Q2206–199N (Pettini *et al.*, 1990, PHSM), Q1101–264, and Q2348–147 were analysed, including a detailed quantitative correction for the line blanketing effect (in which a fraction of otherwise detectable weak lines are obscured by blending in stronger lines). The maximum likelihood values of the column density power law index β were all consistent with each other, with the tightest constraint placed by the Q2348–147 data with $\beta = 1.55 \pm 0.07$.

The fitted value of β was inconsistent with some earlier work, being lower than the best fit values of $\beta \sim 1.7$ of several authors. The value was, however, consistent with the value of Hunstead *et al.* (1987), who used several Lyman series components in the spectrum of Q2000–330 to constrain $N(\text{H I})$ for saturated Lyman α lines. Giallongo *et al.* (1993) pointed out that using saturated lines in an analysis of the $N(\text{H I})$ distribution rendered the result prone to errors. Eliminating saturated lines from their analyses (as was also done in this thesis), they, Cristiani *et al.* (1995), and Songaila *et al.* (1995) found even lower values of β . The low values of Giallongo *et al.*, Cristiani *et al.*, and Songaila *et al.* may be explained by the line blanketing effect, which artificially lowers β when not taken into consideration. The true value of β may therefore be close to 1.5 for $1.5 < z_{\text{abs}} < 3.5$.

The best fitting value of β determined by the present study may be able to explain the observations of Barcons and Webb and Webb *et al.* (1992) (detailed in Section 6.2) *without* requiring small-scale clustering or significant Gunn-Peterson H I absorption at $z_{\text{abs}} \sim 4$, respectively.

Future work on the column density distribution will rely on the increased S/N ratios of data collected with large optical telescopes, such as the 10 m Keck Telescope or the European Southern Observatory's Very Large Telescope. Investigating the $N(\text{H I})$ distribution of saturated Lyman α lines will necessarily involve the observation of higher-order Lyman lines, with spectra extending further to the blue.

9.4 Redshift Evolution

The small sample of QSOs studied in this thesis did not allow a precise determination of the Lyman α cloud redshift evolution parameter γ . The data did, however, allow calculations of γ at high redshift to be compared with values of γ determined by combining *Hubble Space Telescope* (HST) data for the $z_{\text{em}} = 0.16$ QSO 3C 273 (Morris *et al.*, 1991) with the high redshift data. Although this had been done previously, this was the first time the comparison had been made using Lyman α lines of similar rest equivalent widths in both redshift regimes. The result confirmed the conclusion of the earlier work, namely that the rapid rate of Lyman α cloud disappearance seen at $z \gtrsim 2$ slows down appreciably at lower redshifts.

Marginal evidence was presented for a differential rate of evolution between high $N(\text{H I})$ clouds and low $N(\text{H I})$ clouds. Clouds producing Lyman α lines with $W_0 < 100 \text{ m}\text{\AA}$ were found to evolve marginally more slowly than those producing lines with $W_0 \geq 100 \text{ m}\text{\AA}$, over the redshift range $0.01 < z_{\text{abs}} < 2.92$.

An important goal of future work on the redshift evolution of the Lyman α clouds is to fill in the redshift gap between the observations of 3C 273 and higher redshift QSOs. At $z_{\text{abs}} \lesssim 1.5$ (wavelengths $\lambda \lesssim 3000 \text{ \AA}$), the atmosphere becomes increasingly opaque to the redshifted Lyman α photons. The use of a space-based telescope is necessary to investigate redshifts $0.0 < z_{\text{abs}} < 1.5$. Unfortunately, the Goddard High Resolution Spectrograph on the HST is not sensitive enough to record the spectrum of more than a handful of low- z_{em} QSOs within an acceptable observing time. More high-resolution results on low- z_{abs} Lyman α clouds must await the building of a larger space-based telescope.

Failing more low- z_{abs} data, characterisation of the redshift evolution of the Lyman α clouds can be improved by further high-resolution observations of more high- z_{em} QSOs. A larger database will allow the possibility of differential evolution with Lyman α line strength to be examined more closely.

9.5 The Velocity Dispersion Distribution

The distributions of velocity dispersion for the Lyman α lines in the spectra of Q1101–264 and Q2348–147 were analysed and several lines with $b < 20 \text{ km s}^{-1}$ were found. Combined with recent results of Giallongo *et al.* (1993) and Cristiani *et al.* (1995), who also find large numbers of Lyman α lines with $b < 20 \text{ km s}^{-1}$, it appears there is now overwhelming evidence for the existence of Lyman α clouds with inferred temperatures too low to be explained by popular pressure-balanced, photoionisation equilibrium models.

Additionally, there are several lines with $b < 10 \text{ km s}^{-1}$. In one case in the spectrum of Q2348–147 there is a confirming Lyman β line for a saturated Lyman α line, which shows that the line is composed of three components, two with best fit b values of 10 km s^{-1} . Velocity dispersions as low as this pose serious problems for most current models of the Lyman α clouds.

9.5.1 The b - N Correlation

The correlation between b and $\log N$ was investigated for the Lyman α lines in the spectra of Q1101–264 and Q2348–147. In both cases the measured parameters were found to be strongly correlated. However, the correlation for the Q1101–264 data was weaker than that seen in the CNQ data, so no statement could be made on the reality of any intrinsic correlation. The Q2348–147 data, on the other hand, revealed a stronger correlation than that seen in the CNQ data. Since the CNQ b and $\log N$ values were known to be correlated, this implied that the intrinsic b and $\log N$ values for the Lyman α clouds along the sightline to Q2348–147 were also correlated.

Future work on the velocity dispersions of Lyman α lines must consist of higher S/N spectra at the highest resolutions now in use for QSO absorption line studies. Good quality data will hopefully allow the more accurate measurement of b values and end the confusion over the reality of lines with $b < 20 \text{ km s}^{-1}$. Ideally, good quality data of the Lyman β region will allow the positive identification of narrow H I lines, or else show that such lines are more likely to be metal lines.

9.6 Lyman α Cloud Models and Populations

The combined results of the redshift distribution, velocity dispersion distribution, and b - N correlation studies do not support pressure-balanced equilibrium models of the Lyman α clouds such as those of SYBT, Rees (1986), or Ostriker *et al.* (1988). In contrast, they point towards non-equilibrium models such as that of Petitjean *et al.* (1993a), in which the outer regions of the clouds are cooled by adiabatic expansion.

The results of the present work also indicate that there is probably more than one population of objects which give rise to the Lyman α clouds. The clearest evidence for this stems from the results of Morris *et al.* (1993) and Lanzetta *et al.* (1995), who found, respectively, a clear case of a Lyman α cloud with no associated luminous galaxy, and several Lyman α clouds which were associated with luminous galaxies. Other indicators include: (1) The suggestions of differential redshift evolution with cloud column density; (2) the possibility that the b - N correlation is caused by the different properties of sets of clouds which are either confined or freely expanding; and (3) the finding that low column density clouds may be more strongly clustered than clouds of higher $N(\text{H I})$.

The model of Petitjean *et al.* (1993a) includes several populations of Lyman α clouds in order to explain the details of the observed column density distribution. It seems that this model is the most successful so far at explaining the various properties of the Lyman α forest.

9.7 Lyman α Cloud Clustering

Analyses of the clustering properties of the Lyman α clouds along the sightline to Q1101–264 and Q2348–147 were performed. No evidence was found for a non-random distribution in redshift of the Q2348–147 clouds, but strong evidence was found for structure in the distribution of the clouds along the Q1101–264 line of sight.

There appear to be clusters of Lyman α clouds, of size $\sim 10h^{-1}$ Mpc and separated by $\sim 115h^{-1}$ Mpc, with an overdensity of ~ 3 times the random background distribution, along the sightline to Q1101–264. Furthermore, most of the signal seen in the two-point correlation function arises from clouds producing Lyman α lines with $W_0 < 89 \text{ m}\text{\AA}$. A possible explanation for this is that the clouds with low $N(\text{H I})$ trace regions of intergalactic space with relatively low background ionising flux—because high flux would tend to ionise such clouds, rendering them undetectable—and so collect in the voids of the large-scale galaxy distribution.

In a separate analysis, it was shown that the common assumption that a single QSO sightline is representative of the early universe as a whole is likely to be invalid. Thus, although it has been established that clustering exists along the line of sight to one QSO (Q1101–264), it cannot be inferred that clustering on similar scales is a general property of the high-redshift universe. However, neither can it be concluded from a lack of evidence for clustering along other sightlines that no such clustering exists.

Future research on the clustering properties of the Lyman α clouds is likely to be fruitful, for whatever results are achieved will provide constraints on the formation of structure and of galaxies in the early universe. Again, new work should ideally concentrate on obtaining high-resolution spectra of the Lyman α forest at the highest practicable S/N ratios.

9.8 Possible QSO Emission Line Structure

It was noted that the echelle spectra of Q2206–199N (PHSM), Q1101–264, and Q2348–147 all contain unusual “lumpy” features in the wings of the Lyman α emission line. This structure was not seen anywhere else in the spectra, nor in the CNQ spectrum. The hypothesis that these features are not caused by Lyman α forest absorption was investigated. Two possible alternative explanations for the observed features were proposed: (1) That they were caused by absorption in outflowing gas from the QSO environment; (2) that they were intrinsic to the Lyman α emission line.

The hypothesis that the unusual features were intrinsic to the emission line was found to be a viable explanation, consistent with previous observations and current models of the QSO broad emission line region (BLR). A test of this hypothesis was proposed, with predictions based on high-resolution observations of the red wing of the Lyman α emission line and the wings of other broad emission lines. These tests

provide an avenue for future work on the shapes of broad emission lines and lead naturally to more detailed studies of the conditions in QSO BLRs than have yet been carried out.

Bibliography

- Anders, E. and Grevesse, N., 1989, *Geochim. Cosmochim. Acta*, **53**, 197–214.
- Atwood, B., Baldwin, J. A., and Carswell, R. F., 1982, *Ap. J.*, **257**, 559–569.
- Atwood, B., Baldwin, J. A., and Carswell, R. F., 1985, *Ap. J.*, **292**, 58–71.
- Bahcall, J. N., Bergeron, J., Boksenberg, A., Hartig, G. F., Jannuzi, B. T., Kirhakos, S., Sargent, W. L. W., Savage, B. D., Schneider, D. P., Turnshek, D. A., Weymann, R. J., and Wolfe, A. M., 1993, *Ap. J. Suppl.*, **87**, 1–43.
- Bahcall, J. N., 1975, *Ap. J. (Letters)*, **200**, L1–L3.
- Bahcall, N. A., 1988, *Ann. Rev. Astr. and Ap.*, **26**, 631–686.
- Bajtlik, S., Duncan, R. C., and Ostriker, J. P., 1988, *Ap. J.*, **327**, 570–583.
- Baldwin, J. A. and Netzer, H., 1978, *Ap. J.*, **226**, 1–20.
- Barcons, X. and Webb, J. K., 1991, *Mon. Not. R. Astron. Soc.*, **253**, 207–211.
- Baron, E., Carswell, R. F., Hogan, C. J., and Weymann, R. J., 1989, *Ap. J.*, **337**, 609–616.
- Barrow, J. D., Bhavsar, S. P., and Sonoda, D. H., 1984, *Mon. Not. R. Astron. Soc.*, **210**, 19P–23P.
- Bechtold, J. and Schectman, S. A., 1989, in *Active Galactic Nuclei*, edited by D. E. Osterbrock and S. J. Miller, pp. 549–554, Kluwer, Dordrecht.
- Bechtold, J., Weymann, R. J., Lin, Z., and Malkan, M. A., 1987, *Ap. J.*, **315**, 180–197.
- Bechtold, J., Crotts, A. P. S., Duncan, R. C., and Fang, Y., 1994, *Ap. J. (Letters)*, **437**, L83–L86.
- Bechtold, J., 1987, in *High Redshift and Primeval Galaxies*, edited by J. Bergeron, D. Kunth, B. Rocca-Volmerange, and J. Tran Thanh Van, pp. 397–416, Editions Frontières, Gif-sur-Yvette.
- Bechtold, J., 1990, in *ASP Conf. Ser. 10: Evolution of the Universe of Galaxies*, edited by R. G. Kron, pp. 234–244, Astronomical Society of the Pacific, San Francisco.
- Bechtold, J., 1994, *Ap. J. Suppl.*, **91**, 1–78.

- Bessell, M. S. and Pettini, M., 1991, *UCLES Spectrum of the Thorium-Argon Hollow-Cathode Lamp. I. 79 Grooves mm⁻¹ Echelle Grating and IPCS Detector, AAO User Manual 28.1*, Technical Report, Anglo-Australian Observatory.
- Bi, H., Börner, G., and Chu, Y., 1989, *Astr. Ap.*, **218**, 19–23.
- Black, J. H., 1981, *Mon. Not. R. Astron. Soc.*, **197**, 553–563.
- Blandford, R. D. and McKee, C. F., 1982, *Ap. J.*, **255**, 419–439.
- Boissé, P. and Bergeron, J., 1985, *Astr. Ap.*, **145**, 59–69.
- Bond, J. R., Szalay, A. S., and Silk, J., 1988, *Ap. J.*, **324**, 627–638.
- Brotherton, M. S., Wills, B. J., Steidel, C. C., and Sargent, W. L. W., 1994, *Ap. J.*, **423**, 131–142.
- Burbidge, G. R., Crowne, A. H., and Smith, H. E., 1977, *Ap. J. Suppl.*, **33**, 113–188.
- Capriotti, E., Foltz, C., and Byard, P., 1981, *Ap. J.*, **245**, 396–405.
- Carswell, R. F. and Rees, M. J., 1987, *Mon. Not. R. Astron. Soc.*, **224**, 13P–16P.
- Carswell, R. F., Whelan, J. A. J., Smith, M. G., Boksenberg, A., and Tytler, D., 1982, *Mon. Not. R. Astron. Soc.*, **198**, 91–110.
- Carswell, R. F., Morton, D. C., Smith, M. G., Stockton, A. N., Turnshek, D. A., and Weymann, R. J., 1984, *Ap. J.*, **278**, 486–498.
- Carswell, R. F., Webb, J. K., Baldwin, J. A., and Atwood, B., 1987, *Ap. J.*, **319**, 709–722.
- Carswell, R. F., Lanzetta, K. M., Parnell, H. C., and Webb, J. K., 1991, *Ap. J.*, **371**, 36–48.
- Cecil, G., Bland, J., and Tully, R. B., 1990, *Ap. J.*, **355**, 70–87.
- Chaffee, F. H., Weymann, R. J., Latham, D., and Strittmatter, P. A., 1983, *Ap. J.*, **267**, 12–17.
- Chaffee, F. H., Foltz, C. B., Röser, H.-J., Weymann, R. J., and Latham, D. W., 1985, *Ap. J.*, **292**, 362–370.
- Chaffee, F. H., Foltz, C. B., Bechtold, J., and Weymann, R. J., 1986, *Ap. J.*, **301**, 116–123.
- Chernomordik, V. V., 1995, *Ap. J.*, **440**, 431–434.
- Cowie, L. L., Songaila, A., Kim, T.-S., and Hu, E. M., 1995, *Ap. J.*, **000**, 000–000.
- Cristiani, S., D’Odorico, S., Fontana, A., Giallongo, E., and Savaglio, S., 1995, *Mon. Not. R. Astron. Soc.*, **273**, 1016–1032.
- Crotts, A. P. S., 1985, *Ap. J.*, **298**, 732–742.
- Crotts, A. P. S., 1987, *Mon. Not. R. Astron. Soc.*, **228**, 41P–45P.
- Crotts, A. P. S., 1989, *Ap. J.*, **336**, 550–571.

- Davenhall, A. C. and Pettini, M., 1984, *ALAS: Absorption Line Analysis System, A User's Guide*, Technical Report, Royal Greenwich Observatory.
- Davenhall, A. C. and Pettini, M., 1989, *APIG: Absorption Profiles in the Interstellar Gas, A User's Guide*, Technical Report, Royal Greenwich Observatory.
- Davidson, A. F., Kriss, G. A., Ferguson, H. C., Blair, W. P., Bowers, C. W., Dixon, W. V., Durrance, S. T., Feldman, P. D., Henry, R. C., Kimble, R. A., Kruk, J. W., Long, K. S., Moos, H. W., and Vancura, O., 1991, *Nature*, **351**, 128–130.
- de Lapparent, V., Geller, M. J., and Huchra, J. P., 1986, *Ap. J. (Letters)*, **302**, L1–L5.
- de Lapparent, V., Geller, M. J., and Huchra, J. P., 1988, *Ap. J.*, **332**, 45–56.
- Dietrich, M., Kollatschny, W., Peterson, B. M., Bechtold, J., Bertram, R., Bochkarev, N. G., Boroson, T. A., Carone, T. E., Elvis, M., Filippenko, A. V., Gaskell, C. M., Huchra, J. P., Hutchings, J. B., Koratkar, A. P., Korista, K. T., Lame, N. J., Laor, A., MacAlpine, G. M., Malkan, G. M., Mendes de Oliveira, C., Netzer, H., Penfold, J., Penston, M. V., Pérez, E., Pogge, R. W., Richmond, M. W., Rosenblatt, E. I., Shapovalova, A. I., Shields, J. C., Smith, H. A., Smith, P. S., Sun, W.-H., Thiele, U., Veilleux, S., Wagner, R. M., Wilkes, B. J., Wills, B. J., and Wills, D., 1993, *Ap. J.*, **408**, 416–427.
- Dinshaw, N., Impey, C. D., Foltz, C. B., Weymann, R. J., and Chaffee, F. H., 1994, *Ap. J. (Letters)*, **437**, L87–L90.
- Dobrzycki, A. and Bechtold, J., 1991, *Ap. J. (Letters)*, **377**, L69–L72.
- Donahue, M. and Shull, J. M., 1991, *Ap. J.*, **383**, 511–523.
- Duncan, R. C., Ostriker, J. P., and Bajtlik, S., 1989, *Ap. J.*, **345**, 39–51.
- Duncan, R. C., Vishniac, E. T., and Ostriker, J. P., 1991, *Ap. J. (Letters)*, **368**, L1–L4.
- Efron, B. and Tibshirani, R., 1986, *Statistical Science*, **1**, 54–77.
- Elowitz, R. M., Green, R. F., and Impey, C. D., 1995, *Ap. J.*, **440**, 458–465.
- Espey, B. R., Carswell, R. F., Bailey, J. A., Smith, M. G., and Ward, M. J., 1989, *Ap. J.*, **342**, 666–676.
- Fabian, A. C., Naylor, T., and Sciamia, D. W., 1991, *Mon. Not. R. Astron. Soc.*, **249**, 21P–23P.
- Ferland, G. J. and Netzer, H., 1979, *Ap. J.*, **229**, 274–290.
- Ferland, G. J. and Netzer, H., 1983, *Ap. J.*, **264**, 105–113.
- Ferland, G. J. and Truran, J. W., 1981, *Ap. J.*, **244**, 1022–1032.
- Fischer, P., Tyson, J. A., Bernstein, G. M., and Guhathakurta, P., 1994, *Ap. J.*, **431**, L71–L74.
- Foltz, C. B., Weymann, R. J., Röser, H.-J., and Chaffee, Jr., F. H., 1984, *Ap. J. (Letters)*, **281**, L1–L4.

- Francis, P. J., Hewitt, P. C., Foltz, C. B., Chaffee, F. H., Weymann, R. J., and Morris, S. L., 1991, *Ap. J.*, **373**, 465–470.
- Gaskell, C. M., 1982, *Ap. J.*, **263**, 79–86.
- Giallongo, E., Cristiani, S., and Trèvese, D., 1992, *Ap. J. (Letters)*, **398**, L9–L12.
- Giallongo, E., Cristiani, S., Fontana, A., and Trèvese, D., 1993, *Ap. J.*, **416**, 137–149.
- Giallongo, E., D’Odorico, S., Fontana, A., McMahon, R. G., Savaglio, S., Cristiani, S., Molaro, P., and Trèvese, D., 1994, *Ap. J. (Letters)*, **425**, L1–L4.
- Giallongo, E., 1991, *Mon. Not. R. Astron. Soc.*, **251**, 541–544.
- Gunn, J. E. and Peterson, B. A., 1965, *Ap. J.*, **142**, 1633–1636.
- Heisler, J., Hogan, C. J., and White, S. D. M., 1989, *Ap. J.*, **347**, 52–58.
- Hewitt, A. and Burbidge, G., 1993, *Ap. J. Suppl.*, **87**, 451–947.
- Hogan, C. J., 1987, *Ap. J. (Letters)*, **316**, L59–L61.
- Hollander, M. and Wolfe, D. A., 1973, *Nonparametric Statistical Methods*, John Wiley and Sons, New York.
- Howarth, I. D., Murray, J., and Mills, D., 1993, *DIPSO—A friendly spectrum analysis program, Starlink User Note 50.14*, Technical Report, Rutherford Appleton Laboratory.
- Hunstead, R. W., Pettini, M., Blades, J. C., and Murdoch, H. S., 1987, in *IAU Symp. 124: Observational Cosmology*, edited by A. Hewitt, G. Burbidge, and L. Fang, pp. 799–802, Reidel, Dordrecht.
- Hunstead, R. W., Mar, D. P., and Pettini, M., 1995, *J. Astrophys. Astr.*, **16**, 103–110.
- Hunstead, R. W., 1988, in *QSO Absorption Lines: Probing the Universe*, edited by J. C. Blades, D. Turnshek, and N. C., pp. 71–90, Cambridge University Press, Cambridge.
- Ikeuchi, S. and Ostriker, J. P., 1986, *Ap. J.*, **301**, 522–543.
- Jenkins, E. B. and Ostriker, J. P., 1991, *Ap. J.*, **376**, 33–42.
- Korista, K. T., 1992, *Ap. J. Suppl.*, **79**, 285–301.
- Kovner, I. and Rees, M. J., 1989, *Ap. J.*, **345**, 52–58.
- Lanzetta, K. M., Bowen, D. V., Tytler, D., and Webb, J. K., 1995, *Ap. J.*, **442**, 538–638.
- Liu, X. D. and Jones, B. J. T., 1988, *Mon. Not. R. Astron. Soc.*, **230**, 481–490.
- Lowrance, J. L., Morton, D. C., Zucchino, P., Oke, J. B., and Schmidt, M., 1972, *Ap. J.*, **171**, 233–251.
- Lu, L., Wolfe, A. M., and Turnshek, D. A., 1991, *Ap. J.*, **367**, 19–36.

- Lu, L., 1991, *Ap. J.*, **379**, 99–106.
- Lucey, J. and Taylor, K., 1983, *IPCS User's Manual, AAO User Manual 10*, Technical Report, Anglo-Australian Observatory.
- Lynds, R., 1971, *Ap. J. (Letters)*, **164**, L73–L78.
- Lynds, R., 1972, in *IAU Symp. 44: External Galaxies and Quasi-Stellar Objects*, edited by D. S. Evans, pp. 127–138, Reidel, Dordrecht.
- Mar, D. P. and Bailey, G., 1995, *P. A. S. A.*, **12**, (2), 239–243.
- McLeod, B., Rieke, M., and Weedman, D., 1994, *Ap. J.*, **433**, 528–532.
- Meiksin, A. and Madau, P., 1993, *Ap. J.*, **412**, 34–55.
- Meiksin, A., 1994, *Ap. J.*, **431**, 109–122.
- Miralda-Escudé, J. and Ostriker, J. P., 1992, *Ap. J.*, **392**, 15–22.
- Miralda-Escudé, J. and Rees, M. J., 1993, *Mon. Not. R. Astron. Soc.*, **260**, 617–624.
- Mo, H. J., Jing, Y. P., and Börner, G., 1992a, *Ap. J.*, **392**, 452–457.
- Mo, H. J., Xia, X. Y., Deng, Z. G., Börner, G., and Fang, L. Z., 1992b, *Astr. Ap.*, **256**, L23–L26.
- Mo, H. J., Deng, Z. G., Xia, X. Y., Schiller, P., and Börner, G., 1992c, *Astr. Ap.*, **257**, 1–10.
- Monk, A. S., Pettini, M., Penston, M. V., and Blades, J. C., 1995, in preparation.
- Morris, S. L. and van den Bergh, S., 1994, *Ap. J.*, **427**, 696–699.
- Morris, S. L., Weymann, R. J., Savage, B. D., and Gilliland, R. L., 1991, *Ap. J. (Letters)*, **377**, L21–L24.
- Morris, S. L., Weymann, R. J., Dressler, A., McCarthy, P. J., Smith, B. A., Terrile, R. J., Giovanelli, R., and Irwin, M., 1993, *Ap. J.*, **419**, 524–540.
- Morton, D. C., York, D. G., and Jenkins, E. B., 1988, *Ap. J. Suppl.*, **68**, 449–461.
- Murdoch, H. S., Hunstead, R. W., Pettini, M., and Blades, J. C., 1986, *Ap. J.*, **309**, 19–32.
- Norris, J., Hartwick, F. D. A., and Peterson, B. A., 1983, *Ap. J.*, **273**, 450–457.
- Oke, J. B. and Korycansky, D. G., 1982, *Ap. J.*, **255**, 11–19.
- Osmer, P. S. and Smith, M. G., 1977, *Ap. J.*, **213**, 607–618.
- Osterbrock, D. E. and Matthews, W. G., 1986, *Ann. Rev. Astr. and Ap.*, **24**, 171–203.
- Ostriker, J. P., Bajtlik, S., and Duncan, R. C., 1988, *Ap. J. (Letters)*, **327**, L35–L39.
- Parnell, H. C. and Carswell, R. F., 1988, *Mon. Not. R. Astron. Soc.*, **230**, 491–495.
- Peebles, P. J. E., 1980, *The Large Scale Structure of the Universe*, Princeton University Press, Princeton.

- Peterson, B. M., Reichart, G. A., Korista, K. T., and Wagner, R. M., 1990, *Ap. J.*, **352**, 68–80.
- Peterson, B. M., 1993, *Pub. A. S. P.*, **105**, 247–268.
- Peterson, B. M., 1995, in *ASP Conf. Ser. 69: Reverberation Mapping of the Broad-Line Region in Active Galactic Nuclei*, edited by P. M. Gondhalekar, K. Horne, and B. M. Peterson, pp. 1–22, Astronomical Society of the Pacific, San Francisco.
- Petitjean, P. and Bergeron, J., 1990, *Astr. Ap.*, **231**, 309–326.
- Petitjean, P., Bergeron, J., and Puget, J. L., 1992, *Astr. Ap.*, **265**, 375–395.
- Petitjean, P., Bergeron, J., Carswell, R. F., and Puget, J. L., 1993a, *Mon. Not. R. Astron. Soc.*, **260**, 67–76.
- Petitjean, P., Webb, J. K., Rauch, M., Carswell, R. F., and Lanzetta, K., 1993b, *Mon. Not. R. Astron. Soc.*, **262**, 499–505.
- Pettini, M., Hunstead, R. W., Smith, L. J., and Mar, D. P., 1990, *Mon. Not. R. Astron. Soc.*, **246**, 545–564.
- Pettini, M., Smith, L. J., Hunstead, R. W., and King, D. L., 1994, *Ap. J.*, **426**, 79–96.
- Pettini, M., Lipman, K., and Hunstead, R. W., 1995, *Ap. J.*, in press.
- Phillips, S. and Ellis, R. S., 1983, *Mon. Not. R. Astron. Soc.*, **204**, 493–506.
- Pierre, M., Shaver, P. A., and Iovino, A., 1988, *Astr. Ap.*, **197**, L3–L6.
- Press, W. H., Flannery, B. P., Teukolsky, S. A., and Vetterling, W. T., 1988, *Numerical Recipes in C*, Cambridge University Press, Cambridge.
- Rauch, M., Carswell, R. F., Chaffee, F. H., Foltz, C. B., Webb, J. K., Weymann, R. J., Bechtold, J., and Green, R. F., 1992, *Ap. J.*, **390**, 387–404.
- Rauch, M., Carswell, R. F., Webb, J. K., and Weymann, R. J., 1993, *Mon. Not. R. Astron. Soc.*, **260**, 589–609.
- Rees, M. J., 1986, *Mon. Not. R. Astron. Soc.*, **218**, 25P–30P.
- Rice, J. A., 1988, *Mathematical Statistics and Data Analysis*, Wadsworth & Brooks/Cole Advanced Books & Software, Pacific Grove.
- Robertson, J. G., 1986, *Pub. A. S. P.*, **98**, 1220–1231.
- Robinson, R. D., Diego, F., Fish, A. C., Lupton, W. F., Pettini, M., and Walker, D. D., 1989, *The UCL Echelle Spectrograph, AAO User Manual 25.1*, Technical Report, Anglo-Australian Observatory.
- Robinson, R. D., 1985, *The RGO Spectrograph, AAO User Manual 2.2*, Technical Report, Anglo-Australian Observatory.
- Sargent, W. L. W., Young, P. J., Boksenberg, A., and Tytler, D., 1980, *Ap. J. Suppl.*, **42**, 41–81.
- Sargent, W. L. W., Young, P. J., and Schneider, D., 1982, *Ap. J.*, **256**, 374–385.

- Sargent, W. L. W., Boksenberg, A., and Steidel, C. C., 1988, *Ap. J. Suppl.*, **68**, 539–641.
- Sargent, W. L. W., Steidel, C. C., and Boksenberg, A., 1989, *Ap. J. Suppl.*, **69**, 703–761.
- Sargent, W. L. W., 1977, in *The Evolution of Galaxies and Stellar Populations*, edited by B. M. Tinsley and R. B. Larson, pp. 427–444, Yale University Observatory, New Haven.
- Savage, A., Bolton, J. G., Tritton, K. P., and Peterson, B. A., 1978, *Mon. Not. R. Astron. Soc.*, **183**, 473–477.
- Schmidt, M. and Green, R. F., 1983, *Ap. J.*, **269**, 352–374.
- Schmidt, M., 1963, *Nature*, **197**, 1040–1040.
- Schmidt, M., 1965, *Ap. J.*, **141**, 1295–1300.
- Sciama, D. W., 1991, *Ap. J.*, **367**, L39–L41.
- Shaver, P. A. and Robertson, J. G., 1983, *Ap. J.*, **268**, L57–L61.
- Shortridge, K., 1990, *SERC Starlink User Note 86*, Technical Report, Rutherford Appleton Laboratory.
- Smette, A., Surdej, J., Shaver, P. A., Foltz, C. B., Chaffee, Jr., F. H., Weymann, R. J., and Magain, P., 1992, *Ap. J.*, **389**, 39–62.
- Smette, A., Robertson, J. G., Shaver, P. A., Reimers, D., Wisotzki, L., and Köhler, T., 1995, *Astr. Ap.*, in press.
- Smith, M. G., Carswell, R. F., Whelan, J. A. J., Wilkes, B. J., Boksenberg, A., Clowes, R. G., Savage, A., Cannon, R. D., and Wall, J. V., 1981, *Mon. Not. R. Astron. Soc.*, **195**, 437–449.
- Songaila, A., Hu, E. M., and Cowie, L. L., 1995, *Nature*, **375**, 124–126.
- Spitzer, Jr., L., 1978, *Physical Processes in the Interstellar Medium*, John Wiley and Sons, New York.
- Srianand, R. and Khare, P., 1994, *Mon. Not. R. Astron. Soc.*, **271**, 81–93.
- Stathakis, R. A., Hunstead, R. W., Johnston, H., and Robinson, R. D., 1986, *Guides to Wavelength Identification for Comparison Lamps Used with the AAT Spectrograph, AAO User Manual 4.1*, Technical Report, Anglo-Australian Observatory.
- Steidel, C. C. and Sargent, W. L. W., 1987, *Ap. J. (Letters)*, **318**, L11–L13.
- Steidel, C. C. and Sargent, W. L. W., 1990, *Astron. J.*, **99**, 1693–1699.
- Steidel, C. C. and Sargent, W. L. W., 1991, *Astron. J.*, **102**, 1610–1626.
- Stirpe, G. M. and de Bruyn, A. G., 1991, *Astr. Ap.*, **245**, 355–370.
- Stirpe, G. M., de Bruyn, A. G., and van Gronigen, E., 1988, *Astr. Ap.*, **200**, 9–16.
- Trèvese, D., Giallongo, E., and Camurani, L., 1992, *Ap. J.*, **398**, 491–494.

- Turnshek, D. A., Weymann, R. J., Liebert, J. W., Williams, R. E., and Strittmatter, P. A., 1980, *Ap. J.*, **238**, 488–498.
- Tytler, D. and Fan, X.-M., 1994, *Ap. J. (Letters)*, **424**, L87–L90.
- Tytler, D., Fan, X.-M., Burles, S., Cottrell, L., Davis, C., Kirkman, D., and Zuo, L., 1995, in *QSO Absorption Lines*, edited by G. Meylan, pp. 289–298, Springer-Verlag, Berlin.
- Tytler, D., 1987a, *Ap. J.*, **321**, 49–68.
- Tytler, D., 1987b, *Ap. J.*, **321**, 69–79.
- Veilleux, S. and Zheng, W., 1991, *Ap. J.*, **377**, 89–99.
- Vila-Costas, M. B. and Edmunds, M. G., 1993, *Mon. Not. R. Astron. Soc.*, **265**, 199–212.
- Walker, D. D. and Diego, F., 1985, *Mon. Not. R. Astron. Soc.*, **217**, 355–365.
- Walker, T. P., Steigman, G., Schramm, D. N., Olive, K. A., and Kang, H., 1991, *Ap. J.*, **376**, 51–70.
- Wamsteker, W., Rodríguez-Pascual, P., Wills, B. J., Netzer, H., Wills, D., Gilmozzi, R., Barylak, M., Talavera, A., Maoz, D., Barr, P., and Heck, A., 1990, *Ap. J.*, **354**, 446–467.
- Webb, J. K. and Barcons, X., 1991, *Mon. Not. R. Astron. Soc.*, **250**, 270–277.
- Webb, J. K., Barcons, X., Carswell, R. F., and Parnell, H. C., 1992, *Mon. Not. R. Astron. Soc.*, **255**, 319–324.
- Webb, J. K., 1987, in *IAU Symp. 124: Observational Cosmology*, edited by A. Hewitt, G. Burbidge, and L. Fang, pp. 803–806, Reidel, Dordrecht.
- Webb, J. K., 1989, *Nature*, **338**, 620–621.
- Weedman, D. W., 1976, *Q. J. R. Astron. Soc.*, **17**, 227–262.
- Weedman, D. W., 1986, *Quasar Astronomy*, Cambridge University Press, Cambridge.
- Weymann, R. J. and Foltz, C. B., 1983, *Ap. J. (Letters)*, **272**, L1–L4.
- Weymann, R. J., Carswell, R. F., and Smith, M. G., 1981, *Ann. Rev. Astr. and Ap.*, **19**, 41–76.
- Whittle, M., 1985, *Mon. Not. R. Astron. Soc.*, **213**, 1–31.
- Williger, G. M., Carswell, R. F., Webb, J. K., Boksenberg, A., and Smith, M. G., 1989, *Mon. Not. R. Astron. Soc.*, **237**, 635–652.
- Williger, G. M., Baldwin, J. A., Carswell, R. F., Cooke, A. J., Hazard, C., Irwin, M. J., McMahon, R. G., and Storrie-Lombardi, L. J., 1994, *Ap. J.*, **428**, 574–590.
- Wills, B. J., Brotherton, M. S., Fang, D., Steidel, C. C., and Sargent, W. L. W., 1993, *Ap. J.*, **415**, 563–579.

Working Group on Designations from Commission 5 of the IAU, 1991, *Ap. and S. S.*, **183**, 163–165.

Young, P. J., Sargent, W. L. W., Boksenberg, A., Carswell, R. F., and Whelan, J. A. J., 1979, *Ap. J.*, **229**, 891–908.

Young, P. J., Sargent, W. L. W., and Boksenberg, A., 1982, *Ap. J.*, **252**, 10–31.